

# Strong connection between single-particle and density excitations in Bose–Einstein condensates

Shohei Watabe

*Department of Physics, Faculty of Science Division I,  
Tokyo University of Science, Shinjuku, Tokyo, 162-8601, Japan*

## Abstract

Strong connection between the single-particle excitation and the collective excitation stands out as one of the features of Bose–Einstein condensates (BECs). We discuss theoretically these single-particle and density excitations of BECs focusing on the exact properties of the one-body and two-body Green’s functions developed by Gavoret and Nozières. We also investigate these excitations by using the many-body approximation theory at nonzero temperatures. First, we revisited the earlier study presented by Gavoret and Nozières, involving the subsequent results given by Nepomnyashchii and Nepomnyashchii, in terms of the matrix formalism representation. This matrix formalism is an extension of the Nambu representation for the single-particle Green’s function of BECs to discuss the density and current response functions efficiently. We describe the exact low-energy properties of the correlation functions and the vertex functions, and discuss the correspondence of the spectra between the single-particle excitation and the density excitation in the low-energy and low-momentum limits at  $T = 0$ . After deriving the exact low-energy structures of the one-body and two-body Green’s functions, we develop a many-body approximation theory of BECs with making the use of the matrix formalism for describing the single-particle Green’s function and the density response function at nonzero temperatures. We show how the peaks of the single-particle spectral function and the density response function behave with an increasing temperature. Many-body effect on the single-particle spectral function and the density response function is included within a random phase approximation, where satellite structures emerge because of beyond-mean-field effects. Brief comments are also made on recent theories casting doubt upon the conventional wisdom of the BEC: the equivalence of the dispersion relations between the single-particle excitation and the collective excitation in the low-energy and low-momentum regime.

## I. INTRODUCTION

One of the motives for the study of the condensed matter physics is to know excitations in a quantum many-body system, which provides deep understandings of physics behind the system [1–4]. Various kinds of response functions, such as the single-particle spectral function, density response function, pair-correlation function and spin response function, are useful to understand excitations including the single-particle excitation, density excitation, pair-breaking, and spin excitation. Generally, even if the two-body correlation function is constructed from the one-body correlation function, the peak structure of the single-particle excitation does not directly clearly emerge as the exact same peak structure of the density response function generated from the two-body correlation function, where effect of the single-particle excitation may emerge as the broad continuum [1–4]. In contrast to this wisdom, Bose–Einstein condensates (BECs) is of particular interest, since the single-particle property strongly relates to the collective property [5]. The Josephson sum-rule concludes that the outcome of the coherent flow of particles is related to the single-particle spectral function, which explicitly gives the relation among the superfluid density, the condensate density, and the single-particle Green’s function [6–8]. Gavoret and Nozières also provided the exact result which states that in the low-energy and low-momentum regime at absolute zero temperature, the density response function shares the pole of the single-particle spectral function, and both the single-particle and collective excitations are the phonon, the speed of which is equal to the thermodynamic compressible sound mode [9].

Excitations in the superfluid helium have been studied extensively and intensively [3, 5, 10], including the phonon excitation strongly related to the Landau’s criterion for stability of the superfluid, roton and maxon excitations which gives the minimum and maximum in the dispersion law, and hydrodynamic modes such as the first sound and second sound. The liquid helium is highly correlated system with a large gas parameter, where the Bogoliubov theory cannot be directly applied to compare the experimental results. Ultracold atomic gases with a small gas parameter have been a preferable play ground to test the mean-field theory described by the Gross–Pitaevskii equation [11, 12] and the Bogoliubov theory [13]. Furthermore, the recent experimental realization of the box trap in ultracold gases [14] releases us from the conventional restriction of harmonic trap effects, which opens the study of the quantum many-body physics in a highly controllable uniform system. Through the

significant development of the field of ultracold atomic gases [10, 15–18], Feshbach resonance can be used to tune the interaction strength from the weakly interaction to the strongly interaction [19], the phase contrast image can measure the density fluctuation in the real space [20], and the Bragg spectroscopy can measure the structure factor in the momentum space as well as the energy space [21–23]. The recent experiments of the BEC in the ultracold atomic gases have expanded the scope beyond the mean-field region [24]. The ultracold atomic gases may also serve as an ideal potential platform for directly addressing the strong connection between the single-particle excitation and the density excitation in BECs. On the other hand, several theories have been proposed that cast doubt on the paradigm about the BEC [25–31]: the correspondence between the single-particle excitation and the collective excitation in the low-energy and low-momentum region.

The tour de force by Gavoret and Nozières proves the simple exact property of the BEC at the absolute zero temperature [9]; the density response function shares the pole of the single-particle spectral function, which gives the phonon excitation with the thermodynamic compressible sound speed. To follow their proof, we face two separate tasks; One is to analyze and to relate diagrammatic structures of the ground state energy, self-energy contributions, correlation functions, and vertex functions. The other is to calculate relations of diagrammatic structures obtained in the first task by using identities of Green’s functions, where a few notations were not given in the modern way in the original paper [9]. In this paper, we first revisit the Gavoret–Nozières analysis by introducing a systematic formalism for the BECs. The Bardeen–Cooper–Schrieffer theory for the superconductivity has been well formulated by using the Nambu representation, which successfully discusses the gauge invariance and the Meissner effect in the theory of superconductivity [32, 33]. Although the BEC theory has been also formulated by using the Nambu representation, the theory of density and current correlation functions in the BEC does not fully benefit from the Nambu representation. We reconstruct the BEC theory for the density and current correlation functions given by Gavoret and Nozières by using the matrix formalism with the extension of the Nambu representation to these correlation functions, which can reproduce exact relations efficiently.

Recent work [34] has investigated the multiparticle excitation in ultracold gases by using a many-body approximation, and also studied the energy and momentum dependence of the single-particle excitation as well as the collective excitation at the nonzero temperature.

This earlier study employed the approximation that satisfies exact relations, where the off-diagonal self-energy as well as the density vertex for the density response function vanish in the low-energy and low-momentum limits [35, 36]. However, even if the approximation satisfies these exact identities, which are called the Nepomnyashchii–Nepomnyashchii identity and the zero-frequency density vertex identity, it may not exclude the possibility of the approximation dependence of the results, and it does not guarantee that the approximation reproduces qualitative behaviors as well as quantitative properties of the BEC. In this paper, in addition to the study of the exact properties, we also address the single-particle spectral function and density response function by using the many-body approximation theory at nonzero temperatures. We take the many-body theory different from the earlier paper [34] with focusing on the effect of the vertex corrections, and discuss the qualitative properties common in these approximations.

This paper is structured as follows. Section II introduces the correlation functions of BECs studied in the present paper. Section III describes the relations between the vertex functions in the low-energy regime. Using these results, the low-energy behaviors of the correlation functions at  $T = 0$  are discussed in Sec. IV. The formulation in these sections, where the earlier result by Gavoret and Nozières [9] and the subsequent result by Nepomnyashchii and Nepomnyashchii [35, 36] are revisited, is developed in the matrix formalism. This formalism can efficiently address structures of diagrams and infrared divergences in BECs [34, 37–39], which has been successfully applied to reproduce the Nepomnyashchii–Nepomnyashchii identity [38]. Section V reviews the earlier experimental and theoretical studies focused on the sound mode in the superfluid helium as well as ultracold atomic BECs, where variant sound modes in the superfluid, such as the second sound, are important but beyond the scope of the present paper. This section also serves as comments of recent theories casting doubt upon the paradigm about the BEC: the equivalence of the dispersion relations between the single-particle excitation and the collective excitation in the low-energy and low-momentum regime. Section VI develops the formulation of the random phase approximation in terms of the matrix formalism. Section VII discusses the single-particle spectral function and the density response function at nonzero temperatures within the many-body approximation developed in the previous section VI. This section also addresses the correspondence between peaks of the single-particle spectral function and the density response function, and studies the sound speed estimated from the compressibil-

ity zero-frequency sum-rule by using the density response function obtained in the random phase approximation. We end with the summary and conclusions in Sec. VIII.

Throughout this paper, we set  $\hbar = k_B = 1$ , and take the system volume  $V$  to be unity. The terms,  $n$ -particle irreducible ( $n$ PI) and  $n$ -particle reducible ( $n$ PR), are applied to represent diagrams that cannot and can be separated into two pieces by cutting  $n$  single-particle lines, respectively. The regular part called in this paper means the proper part, which represents a diagram that cannot be separated into two pieces by cutting a single interaction line.

## II. CORRELATION FUNCTIONS

We consider the Hamiltonian of an interacting Bose system with the atomic mass  $m$ , given by

$$\hat{H} = \int d\mathbf{r} \frac{1}{2m} \nabla \hat{\Psi}^\dagger(\mathbf{r}) \nabla \hat{\Psi}(\mathbf{r}) + \frac{1}{2} \int d\mathbf{r} \int d\mathbf{r}' \hat{\Psi}^\dagger(\mathbf{r}) \hat{\Psi}^\dagger(\mathbf{r}') U_{\text{int}}(\mathbf{r} - \mathbf{r}') \hat{\Psi}(\mathbf{r}') \hat{\Psi}(\mathbf{r}), \quad (1)$$

where  $\hat{\Psi}(\mathbf{r})$  and  $\hat{\Psi}^\dagger(\mathbf{r})$  are bosonic annihilator and creator, respectively. In the BEC ordered phase, the field operator may be treated by the so-called Bogoliubov prescription:

$$\hat{\Psi}(\mathbf{r}) = \Phi_0(\mathbf{r}) + \hat{\phi}(\mathbf{r}), \quad (2)$$

where  $\Phi_0(\mathbf{r})$  represents the order parameter of the condensate wave function, and  $\hat{\phi}(\mathbf{r})$  the non-condensate part. In the uniform system with the condensate density  $n_0$ , we may suppose

$$\hat{\Psi}(\mathbf{r}) = \sqrt{n_0} + \sum_{\mathbf{p} \neq 0} \hat{a}_{\mathbf{p}} e^{i\mathbf{p} \cdot \mathbf{r}}, \quad (3)$$

where the condensate wave function is taken to be real, i.e.,  $\Phi_0(\mathbf{r}) = \sqrt{n_0}$ .

We consider a contact interaction  $U_{\text{int}}(\mathbf{r} - \mathbf{r}') = U\delta(\mathbf{r} - \mathbf{r}')$ , where the interaction strength  $U$  is related to the  $s$ -wave scattering length  $a_s$  through the relation  $4\pi a_s/m = U/[1 + U \sum_{\mathbf{p}}^{p_c} 1/(2\varepsilon_{\mathbf{p}})]$ , where  $p_c$  is the cutoff momentum, and  $\varepsilon_{\mathbf{p}}$  the kinetic energy of the bosonic particle  $\varepsilon_{\mathbf{p}} = \mathbf{p}^2/2m$ .

An average of an operator  $\hat{O}$  at temperature  $T$  is given by

$$\langle \hat{O} \rangle = \frac{1}{\Xi} \text{Tr}[e^{(-\hat{H}/T)} \hat{O}]. \quad (4)$$

Here, the Hamiltonian  $\hat{\mathcal{H}}$  with the chemical potential  $\mu$  is given by

$$\hat{\mathcal{H}} = \hat{H} - \mu \int d\mathbf{r} \hat{\phi}^\dagger(\mathbf{r}) \hat{\phi}(\mathbf{r}), \quad (5)$$

where the Bogoliubov prescription is applied to  $\hat{H}$ . The partition function is given by  $\Xi = \text{Tr}[\exp(-\hat{\mathcal{H}}/T)]$ , which may be regarded as the quasi-grand partition function because the term  $-\mu n_0$  is omitted from the hamiltonian  $\hat{\mathcal{H}}$ . It is sufficient to evaluate an average by using  $\exp(-\hat{\mathcal{H}}/T)$  with the Bogoliubov prescription, because the term  $-\mu n_0$  is the  $c$ -number, which is reduced in the form of the average.

We introduce three representations of the single-particle thermal Green's function

$$G(\mathbf{p}, i\omega_n) = - \int_0^{1/T} d\tau e^{i\omega_n \tau} \langle T_\tau \hat{\mathbf{A}}_{\mathbf{p}}(\tau) \hat{\mathbf{A}}_{\mathbf{p}}^\dagger(0) \rangle, \quad (6)$$

$$\mathbf{G}(\mathbf{p}, i\omega_n) = - \int_0^{1/T} d\tau e^{i\omega_n \tau} \langle T_\tau \hat{\mathbf{A}}_{\mathbf{p}}(\tau) \otimes \hat{\mathbf{A}}_{-\mathbf{p}}(0) \rangle, \quad (7)$$

$$\mathbf{G}^\dagger(\mathbf{p}, i\omega_n) = - \int_0^{1/T} d\tau e^{i\omega_n \tau} \langle T_\tau \hat{\mathbf{A}}_{\mathbf{p}}^\dagger(0) \otimes \hat{\mathbf{A}}_{-\mathbf{p}}(\tau) \rangle, \quad (8)$$

where  $\hat{\mathbf{A}}_{\mathbf{p}}(\tau) \equiv (\hat{a}_{\mathbf{p}}(\tau), \hat{a}_{-\mathbf{p}}^\dagger(\tau))^T$  in the Nambu representation [40]. Here,  $\otimes$  is the Kronecker product, and  $T_\tau$  denotes an operation of  $\tau$ -ordering, which arranges operators from right to left in order of increasing the imaginary time  $\tau$ . In the bosonic case, the Matsubara frequency is  $\omega_n = 2\pi nT$  with  $n \in \mathbb{Z}$ . The Green's functions  $G$ ,  $\mathbf{G}$  and  $\mathbf{G}^\dagger$  are  $(2 \times 2)$ ,  $(4 \times 1)$ , and  $(1 \times 4)$ -matrices, respectively.

The Dyson equations for the Green's functions are given by

$$G(p) = G_0(p) + G_0(p) \Sigma(p) G(p), \quad (9)$$

$$\mathbf{G}(p) = \mathbf{G}_0(p) + \{[G_0(p) \Sigma(p)] \otimes \sigma_0\} \mathbf{G}(p), \quad (10)$$

$$\mathbf{G}^\dagger(p) = \mathbf{G}_0^\dagger(p) + \mathbf{G}^\dagger(p) \{\sigma_0 \otimes [\Sigma(-p) G_0(-p)]\}, \quad (11)$$

with  $p = (i\omega_n, \mathbf{p})$ . Each matrix equation provides equivalent equations for the Green's function  $G_{ij}$  with  $i, j = 1, 2$ . Here,  $G_0^{-1}(p) = i\omega_n \sigma_3 - \varepsilon_{\mathbf{p}} + \mu$  is the  $(2 \times 2)$ -matrix Green's function for non-interacting bosons, where  $\sigma_{j=0,1,2,3}$  are the Pauli matrices. The identity matrix of the size 2 is given by  $\sigma_0$ . The non-interacting parts  $\mathbf{G}_0$  and  $\mathbf{G}_0^\dagger$  are given by

$$\mathbf{G}_0(p) = \begin{pmatrix} 0 \\ G^{(0)}(p) \\ G^{(0)}(-p) \\ 0 \end{pmatrix}, \quad \mathbf{G}_0^\dagger(p) = (0, G^{(0)}(p), G^{(0)}(-p), 0), \quad (12)$$

where  $G^{(0)}(p) = 1/(i\omega_n - \varepsilon_{\mathbf{p}} + \mu)$ . Interaction effects are included into the  $(2 \times 2)$ -matrix self-energy  $\Sigma$ , and we may introduce the  $(4 \times 1)$ -matrix self-energy  $\mathbf{\Sigma}$ , and the  $(1 \times 4)$ -matrix self-energy  $\mathbf{\Sigma}^\dagger$ . Diagrammatic representations of matrix elements of  $(G, \mathbf{G}, \mathbf{G}^\dagger)$  as well as  $(\Sigma, \mathbf{\Sigma}, \mathbf{\Sigma}^\dagger)$  are summarized in Appendix A. Matrix elements  $G_{ij}$  are not independent of each other:  $G_{11}(p) = G_{22}(-p)$  and  $G_{12}(p) = G_{21}(p) = G_{12}(-p) = G_{21}(-p)$ , where the self-energies  $\Sigma_{ij}$  satisfy the same relations [1, 9].

The Green's function  $G$  provides the non-condensate density

$$n' = n - n_0 = -\frac{1}{2}T \sum_p \text{Tr}[G(p)e^{\sigma_3 i\omega_n \delta}], \quad (13)$$

where  $n$  is the total particle density. In the following, we omit the convergence factor  $\exp(\sigma_3 i\omega_n \delta)$  for simplicity. The formalism at  $T = 0$  is introduced by applying the analytic continuation ( $i\omega_n \rightarrow \omega + i\delta$ ) as well as the following replacement  $-T \sum_n \rightarrow i \int d\omega/(2\pi)$  [1, 33].

The  $(4 \times 4)$ -matrix two-particle Green's function  $K(p, p'; q)$  is composed of the one-particle reducible (1PR) and one-particle irreducible (1PI) parts, i.e.,  $K^{1\text{PR}}$  and  $K^{1\text{PI}}$ , where the 1PR part is specific to the condensed Bose system. (In Ref. [9], these are called the singular and the regular part, respectively.) The two-particle Green's function  $K$  is given by (See Fig. 1)

$$K(p, p'; q) = K^{1\text{PI}}(p, p'; q) + K^{1\text{PR}}(p, p'; q), \quad (14)$$

where

$$\begin{aligned} K^{1\text{PI}}(p, p'; q) = & K_0(p; q)T^{-1}(\delta_{p, p'} + \hat{T}\delta_{p, -p'-q}) \\ & - K_0(p; q)\Gamma(p, p'; q)K_0(p'; q) \\ & - K_0(p; q)\Gamma(p, -p' - q; q)\hat{T}K_0(p'; q), \end{aligned} \quad (15)$$

$$K^{1\text{PR}}(p, p'; q) = -Q(p; q)G(q)Q^\dagger(p'; q). \quad (16)$$

For the 1PI part,  $K_0$  is a bare part of the  $(4 \times 4)$ -matrix two-particle Green's function

$$K_0(p; q) = G(p+q) \otimes G(-p), \quad (17)$$

and  $\Gamma$  is the  $(4 \times 4)$ -matrix four point vertex, given by (See Fig. 2 (a))

$$\Gamma(p, p'; q) = I(p, p'; q) - T \sum_{p''} I(p, p''; q)K_0(p''; q)\Gamma(p'', p'; q). \quad (18)$$

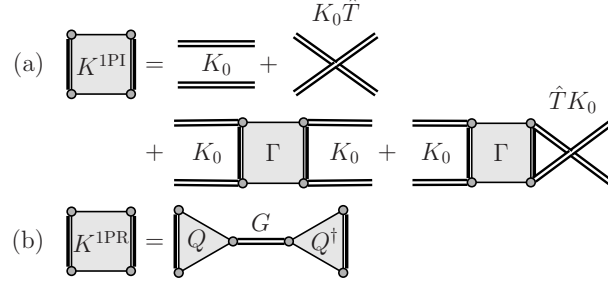


FIG. 1. Two-particle Green's function. (a) One-particle irreducible part  $K^{1PI}$ . (b) One-particle reducible part  $K^{1PR}$ .

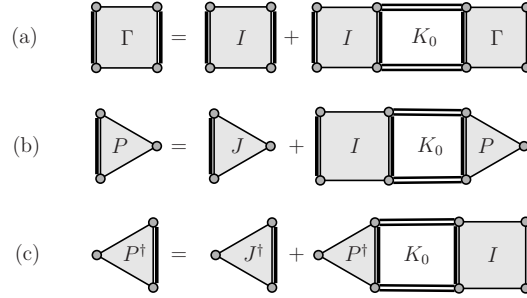


FIG. 2. (a) Bethe-Salpeter equation of the four-point vertex  $\Gamma$ . Here,  $I$  is a two-particle irreducible (2PI) part of the four point vertex. (b) Equation of the three-point vertices  $P$ . (c) Equation of  $P^\dagger$ . Here,  $J$  and  $J^\dagger$  are 2PI parts of the three-point vertices.

Here,  $I(p, p'; q)$  is a two-particle irreducible (2PI) part of the  $(4 \times 4)$ -matrix four point vertex. The matrix  $\hat{T}$  is given by

$$\hat{T} = \begin{pmatrix} 1 & 0 & 0 & 0 \\ 0 & 0 & 1 & 0 \\ 0 & 1 & 0 & 0 \\ 0 & 0 & 0 & 1 \end{pmatrix}, \quad (19)$$

which exchanges upper and lower ends of a two-particle Green's function (See Appendix A).

For the 1PR part, the  $(4 \times 2)$ - and  $(2 \times 4)$ -matrix vertices  $Q$  and  $Q^\dagger$  are given by

$$Q(p; q) = K_0(p; q)P(p; q) + T^{-1}\sqrt{-1}(\delta_{p,0} + \hat{T}\delta_{p,-q})\mathcal{G}_{1/2}, \quad (20)$$

$$Q^\dagger(p; q) = P^\dagger(p; q)K_0(p; q) + T^{-1}\sqrt{-1}\mathcal{G}_{1/2}^\dagger(\delta_{p,0} + \hat{T}\delta_{p,-q}). \quad (21)$$



Here, the  $(4 \times 2)$ - and  $(2 \times 4)$ -matrix three point vertices  $P$  and  $P^\dagger$  are given by (See Figs. 2 (b) and (c))

$$P(p; q) = J(p; q) - T \sum_{p'} I(p, p'; q) K_0(p'; q) P(p'; q), \quad (22)$$

$$P^\dagger(p; q) = J^\dagger(p; q) - T \sum_{p'} P^\dagger(p'; q) K_0(p'; q) I(p', p; q), \quad (23)$$

where  $J$  and  $J^\dagger$  are 2PI parts of  $P$  and  $P^\dagger$ . The condensate contributions here are included by the  $(4 \times 2)$  and  $(2 \times 4)$ -matrix condensate Green's functions

$$\mathcal{G}_{1/2} = \sigma_0 \otimes G_{1/2}, \quad \mathcal{G}_{1/2}^\dagger = \sigma_0 \otimes G_{1/2}^\dagger, \quad (24)$$

where  $G_{1/2}$  and  $G_{1/2}^\dagger$  are the condensate Green's functions

$$G_{1/2} = \sqrt{-1} \begin{pmatrix} \Phi_0 \\ \Phi_0^* \end{pmatrix}, \quad G_{1/2}^\dagger = \sqrt{-1} (\Phi_0^*, \Phi_0). \quad (25)$$

In the case at  $T = 0$ , the factor  $\sqrt{-1}$  is replaced with  $\sqrt{-i}$  [40].

The density and current correlation functions  $\chi_{\mu\nu}(q)$  are defined as

$$\chi_{\mu\nu}(q) = -\frac{1}{4} T^2 \sum_{p, p'} \langle \lambda_\mu(p; q) | K(p, p'; q) | \lambda_\nu(p'; q) \rangle, \quad (26)$$

where the density-density and current-current correlation functions are  $\chi_{00}(q)$  and  $\chi_{ij}(q)$  for  $i, j = 1, 2, 3$ , respectively. Here,  $i, j = 1, 2, 3$  are the index of the Cartesian coordinate. The density-current correlation functions are  $\chi_{0i}(q)$  and  $\chi_{i0}(q)$  for  $i = 1, 2, 3$ . The density and current vertex vector  $|\lambda_\mu(p; q)\rangle$  is given by

$$|\lambda_\mu(p; q)\rangle = \lambda_\mu(p; q) |f_\mu\rangle, \quad (27)$$

where

$$\lambda_\mu(p; q) = \begin{cases} 1 & (\mu = 0) \\ \frac{1}{m} \left( \mathbf{p} + \frac{\mathbf{q}}{2} \right)_i & (\mu = i = 1, 2, 3), \end{cases} \quad (28)$$

and

$$|f_\mu\rangle = \begin{pmatrix} 0 \\ 1 \\ f_\mu \\ 0 \end{pmatrix}, \quad f_\mu = \begin{cases} +1 & (\mu = 0) \\ -1 & (\mu = i = 1, 2, 3). \end{cases} \quad (29)$$

$$\chi_{\mu\nu}^{\text{1PI}} = \frac{1}{2} \times \left[ \langle \lambda_\mu | K_0 | \lambda_\nu \rangle + \langle \lambda_\mu | K_0 \Gamma K_0 | \lambda_\nu \rangle \right]$$

FIG. 3. One-particle irreducible part of the density and current response function  $\chi_{\mu\nu}^{\text{1PI}}$ .

The density vertex vector is simply given by  $|\lambda_0(p; q)\rangle = |f_0\rangle$ .

The correlation functions (26) are constructed from the two-particle Green's function  $K$ , which are decomposed into the 1PI and 1PR parts, giving the form

$$\chi_{\mu\nu}(q) = \chi_{\mu\nu}^{\text{1PI}}(q) + \chi_{\mu\nu}^{\text{1PR}}(q). \quad (30)$$

The 1PI and 1PR parts are of the form (See Fig. 3)

$$\chi_{\mu\nu}^{\text{1PI}}(q) = -\frac{1}{4}T^2 \sum_{p,p'} \langle \lambda_\mu(p; q) | K^{\text{1PI}}(p, p'; q) | \lambda_\nu(p'; q) \rangle, \quad (31)$$

$$\chi_{\mu\nu}^{\text{1PR}}(q) = \Upsilon_\mu^\dagger(q) G(q) \Upsilon_\nu(q), \quad (32)$$

where

$$\Upsilon_\nu(q) = -\frac{1}{2}T \sum_{p'} Q^\dagger(p'; q) | \lambda_\nu(p'; q) \rangle, \quad (33)$$

$$\Upsilon_\mu^\dagger(q) = -\frac{1}{2}T \sum_p \langle \lambda_\mu(p; q) | Q(p; q). \quad (34)$$

### III. RELATIONS BETWEEN VERTEX FUNCTIONS

Vertex functions in the static and zero-momentum limits can be systematically generated from all the possible linked diagrams that construct the thermodynamic potential  $\Omega' = -T \ln \Xi$ . An exact many-line vertex  $M(n_{\text{out}}, n_{\text{in}}, n_U)$  is given by [36]

$$M(n_{\text{out}}, n_{\text{in}}, n_U) = n_0^{(n_{\text{out}} - n_{\text{in}})/2} \times \left( -\frac{\partial}{\partial \mu} \right)_{T, n_0}^{n_U} \left( \frac{\partial}{\partial n_0} \right)_{T, \mu}^{n_{\text{out}}} \left[ n_0^{n_{\text{in}}} \left( \frac{\partial}{\partial n_0} \right)_{T, \mu}^{n_{\text{in}}} \right] \Omega'(T, \mu, n_0). \quad (35)$$

Here,  $n_{\text{in(out)}}$  is the number of incoming (outgoing) particle lines that can connect to the vertex function  $M$ , and  $n_U$  is the number of external interaction lines  $U$  that can also connect to the vertex function  $M$ . The operator  $n_0^{n_{\text{in(out)}/2}} (\partial/\partial n_0)^{n_{\text{in(out)}}$  works as the elimination of

the  $n_{\text{in(out)}}$  condensate lines  $\Phi_0^{(*)}(=\sqrt{n_0})$  from the linked diagrams. The operator  $(-\partial/\partial\mu)^{n_U}$  affects on the Green's function  $G_0$  in the linked diagrams, which provides the  $r_U$  vertex points for the interaction line due to the relation  $-\partial G_0/\partial\mu = G_0^2$ . This prescription was originally invented for the ground state energy at  $T = 0$  [36]. Since the linked diagrammatic structures for the thermodynamic potential at nonzero temperature are formally the same as those of the ground state energy [? ], this prescription is also applied to the nonzero temperature case [64].

The equation (35) generates the self-energy matrix  $\Sigma$ , the three point vertex matrix  $P$ , and the density vertex  $\Upsilon_0$  in the zero-energy and zero-momentum limits, respectively given by

$$\Sigma(0) = \frac{\partial\Omega'}{\partial n_0} \begin{pmatrix} 1 & 0 \\ 0 & 1 \end{pmatrix} + n_0 \frac{\partial^2\Omega'}{\partial n_0^2} \begin{pmatrix} 1 & 1 \\ 1 & 1 \end{pmatrix}, \quad (36)$$

$$P(0;0) = 2\sqrt{n_0} \frac{\partial^2\Omega'}{\partial n_0^2} \eta + n_0^{3/2} \frac{\partial^3\Omega'}{\partial n_0^3} \eta_a, \quad (37)$$

$$\Upsilon_0(0) = \sqrt{n_0} \left( 1 - \frac{\partial^2\Omega'}{\partial\mu\partial n_0} \right) |+\rangle, \quad (38)$$

where  $|\pm\rangle = (1, \pm 1)^T$ ,  $\langle\pm| = (1, \pm 1)$  and

$$\eta = \begin{pmatrix} 1 & 0 \\ 1 & 1 \\ 1 & 1 \\ 0 & 1 \end{pmatrix}, \quad \eta_a = \begin{pmatrix} 1 & 1 \\ 1 & 1 \\ 1 & 1 \\ 1 & 1 \end{pmatrix}. \quad (39)$$

Vertices  $\Sigma$  and  $P$  are related with each other, giving the form

$$P(0;0)|-\rangle = \frac{2}{\sqrt{n_0}} \Sigma_{12}(0) \eta |-\rangle = \frac{2}{\sqrt{n_0}} \hat{A} \Sigma(0), \quad (40)$$

where

$$\hat{A} = \begin{pmatrix} 1 & 0 & 0 & 0 \\ 0 & 0 & 0 & 0 \\ 0 & 0 & 0 & 0 \\ 0 & 0 & 0 & -1 \end{pmatrix}. \quad (41)$$

The thermodynamic potential  $\Omega'$  is related to the grand potential  $\Omega$  by introducing the chemical potential of the condensate  $\mu_0$ . We have the relation  $\Omega = \Omega' - \mu_0 n_0$  with the

condition  $\mu_0 = \mu$  [36]. Since the condensate density is determined from the condition  $\partial\Omega/\partial n_0 = 0$ , we have

$$\mu_0(T, \mu, n_0) = \mu = \frac{\partial\Omega'}{\partial n_0}. \quad (42)$$

Given this relation, we may derive the Hugenholtz-Pines relation  $\Sigma_{11}(0) - \Sigma_{12}(0) = \mu$  [41], or  $\Sigma(0)|-\rangle = \mu|-\rangle$  in the matrix form. The Nepomnyashchii–Nepomnyashchii identity [35, 36], giving the form

$$\Sigma_{12}(0) = n_0 \frac{\partial^2 \Omega'}{\partial n_0^2} = n_0 \left. \frac{\partial \mu_0}{\partial n_0} \right|_{T, \mu} = 0, \quad (43)$$

reduces the Hugenholtz-Pines relation to the following form

$$\Sigma(0) = \mu. \quad (44)$$

The derivation of the Nepomnyashchii–Nepomnyashchii identity with the use of the matrix formalism is summarized in Ref. [38], and physics of this identity can be found in Refs. [5, 35, 36, 38, 39, 42–48]. The Nepomnyashchii–Nepomnyashchii identity  $\Sigma_{12}(0) = 0$  is derived from the relation between vertex functions and the nature of the infrared divergence in the self-energy diagrams [35, 36, 38], and it is strongly related to the weak infrared divergence of the longitudinal susceptibility caused by the convolution of the phase-phase correlation function [38, 42]. As a result, this identity is also valid at nonzero temperature [38, 64]. The identity (43) also provides a relation  $P(0; 0)|-\rangle = 0$ .

The Nepomnyashchii–Nepomnyashchii identity also provides the zero-frequency density vertex identity, i.e., the vanishing density vertex in the limit  $p = 0$ , giving the form

$$\Upsilon_0(0) = 0. \quad (45)$$

This is valid in the isothermal condition, and the derivation is summarized in Appendix B.

In the remaining part of this section, we summarize low-energy behaviors of vertex functions in our matrix representation. We first consider a relation between  $\Sigma$  and  $P$  as well as a relation between  $\mathbf{G}$  and  $L$ , where the  $(4 \times 2)$ -matrix  $L$  (diagrammatically described in Fig. 4) is given by

$$L(p; q) = K_0(p; q)P(p; q). \quad (46)$$

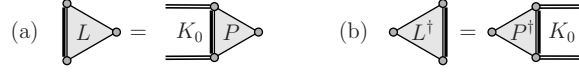


FIG. 4. Three point vertices  $L$  and  $L^\dagger$ .

With respect to  $(\Sigma, P)$  or  $(\mathbf{G}, L)$ , relations at small but finite  $q = (\varpi, \mathbf{q})$  are given by [9]

$$P(p, +q)|0\rangle + P(p, -q)|1\rangle \simeq \hat{\mathcal{D}}(q)\Sigma(p), \quad (47)$$

$$L(p, +q)|0\rangle + L(p, -q)|1\rangle \simeq \hat{\mathcal{D}}(q)\mathbf{G}(p), \quad (48)$$

where  $|0\rangle = (1, 0)^T$ ,  $|1\rangle = (0, 1)^T$  and  $\hat{\mathcal{D}}(q) = \mathcal{D}_1(q) + \hat{B}\mathcal{D}_2(q)$  with

$$\mathcal{D}_1(q) \equiv \frac{1}{\sqrt{n_0}} \left( 2n_0 \frac{\partial}{\partial n_0} + \sum_{\nu=0}^3 q_\nu \frac{\delta}{\delta x_\nu} \right), \quad (49)$$

$$\mathcal{D}_2(q) \equiv \frac{1}{\sqrt{n_0}} \sum_{\nu=0}^3 q_\nu \partial_\nu, \quad (50)$$

$$\hat{B} \equiv \begin{pmatrix} 0 & 0 & 0 & 0 \\ 0 & -1 & 0 & 0 \\ 0 & 0 & +1 & 0 \\ 0 & 0 & 0 & 0 \end{pmatrix}. \quad (51)$$

Here, two types of derivatives are introduced:  $\delta/\delta x_\nu = (\partial/\partial\mu, \delta/\delta\mathbf{p})$  and  $\partial_\nu = (\partial/\partial\omega, \partial/\partial\mathbf{p})$ . The partial derivative  $\partial/\partial p_i$  and the total derivative  $\delta/\delta p_i$  for  $i = 1, 2, 3$  are respectively defined as  $\partial G^{(0)}(\pm\mathbf{p})/\partial p_i \equiv \lim_{dp_i \rightarrow 0} [G^{(0)}(\pm(\mathbf{p} + dp_i \mathbf{e}_i)) - G^{(0)}(\pm\mathbf{p})]/dp_i$ , and  $\delta G^{(0)}(\pm\mathbf{p})/\delta p_i \equiv \lim_{\delta p_i \rightarrow 0} [G^{(0)}(\pm\mathbf{p} + \delta p_i \mathbf{e}_i) - G^{(0)}(\pm\mathbf{p})]/\delta p_i$ , where  $\mathbf{e}_i$  is the unit vector in the Cartesian coordinate [9]. The total derivative  $\delta/\delta p_i$  is related to an observation of the system from a reference frame with a speed  $-\delta\mathbf{p}/m$ . (Details can be found in Sec. V in Ref. [9].)

In the limit  $q = 0$ , (47) and (48) are reduced into

$$\begin{pmatrix} P(p; 0)|+\rangle \\ L(p; 0)|+\rangle \end{pmatrix} = 2\sqrt{n_0} \frac{\partial}{\partial n_0} \begin{pmatrix} \Sigma(p) \\ \mathbf{G}(p) \end{pmatrix}. \quad (52)$$

The three point vertex  $P$  (or  $L$ ) is created from the two-point vertex  $\Sigma$  (or the Green's function  $\mathbf{G}$ ) by eliminating a condensate line from  $\Sigma$  (or  $\mathbf{G}$ ) that provides an extra vertex point at  $q = 0$  [9].

We also have relations [9]

$$\begin{pmatrix} P(p; 0) | - \rangle \\ L(p; 0) | - \rangle \end{pmatrix} = \frac{2}{\sqrt{n_0}} \begin{pmatrix} \hat{A}\Sigma(p) \\ \hat{A}\mathbf{G}(p) \end{pmatrix}. \quad (53)$$

The upper equality in (53) can be derived as follows [9]; The self-energy  $\Sigma$  can be constructed from two parts. One is the three point vertex  $J$ , where one of the three vertex points is blocked by a condensate line  $\sqrt{n_0}$ . The other is the four point vertex  $I$ , where two of the four vertex points are blocked by a Green's function  $G_{12}$  or  $G_{21}$ . It gives the following relation (See Appendix B in Ref [9]):

$$2\hat{A}\Sigma(p) = \sqrt{n_0}J(p; 0) | - \rangle - 2T \sum_{p'} I(p, p'; 0) \hat{A}\mathbf{G}(p'). \quad (54)$$

By comparing Eqs. (22) with (54) with the use of a mathematical identity

$$\hat{A}\mathbf{G}(p) = K_0(p; 0) \hat{A}\Sigma(p), \quad (55)$$

we obtain the first equality of (53), which is consistent with (40) in the limit  $p = 0$ . The second equality in (53) with respect to  $(L, \mathbf{G})$  is also obtained by following the similar way.

According to symmetries, the density and current vertices can be given by

$$\Upsilon_\nu(q) = \begin{pmatrix} \gamma_\nu(q) \\ \gamma_\nu(-q) \end{pmatrix}, \quad \Upsilon_\mu^\dagger(q) = (\gamma_\mu(q), \gamma_\mu(-q)), \quad (56)$$

the matrix element of which in the low-energy regime behaves as (See Appendix D)

$$\gamma_\nu(q) \simeq \sqrt{n_0} \lambda_\nu(0; q) - \frac{1}{4} T \sum_p \lambda_\nu(p, 0) \{ \mathcal{D}_1(q) \text{Tr}[\sigma'_\nu G(p)] - \mathcal{D}_2(q) \text{Tr}[\sigma'_\nu \sigma_3 G(p)] \}. \quad (57)$$

#### IV. LOW ENERGY BEHAVIORS OF CORRELATION FUNCTIONS AT $T = 0$

The self-energy at small  $p$  behaves as [36]

$$\begin{aligned} \Sigma(p) = & \mu + \omega \sigma_3 + \Delta \Sigma(p) \sigma_+ \\ & + \frac{1}{2} \partial_\omega^2 \Sigma'(0) \omega^2 + \frac{1}{2} \partial_{\mathbf{p}}^2 \Sigma'(0) \mathbf{p}^2 + \dots, \end{aligned} \quad (58)$$

where  $\sigma_+ = |+\rangle\langle+|$ . The first term  $\mu$  is to satisfy the Hugenholtz–Pines relation as well as the Nepomnyashchii–Nepomnyashchii identity in (44). The term  $\Delta \Sigma(p)$  is the so-called

non-analytic term [36], which satisfies  $\Delta\Sigma(p) \gg |\mathbf{p}|^2$  as well as  $\Delta\Sigma(p) \gg \omega^2$  at small  $p$ . Note that  $\Delta\Sigma(0) = 0$  as well as  $\Delta\Sigma(-p) = \Delta\Sigma(p)$  hold, because of the Nepomnyashchii–Nepomnyashchii identity  $\Sigma_{12}(0) = 0$  and a symmetry relation  $\Sigma_{12,21}(-p) = \Sigma_{12,21}(p)$ . The symmetry relation  $\Sigma(0, \mathbf{p}) = \Sigma(0, -\mathbf{p})$  also provides the relation  $\partial_{\mathbf{p}}\Sigma'(0) = 0$ , which provides the absence of the first order of  $\mathbf{p}$  in Eq. (58). Here, the self-energy  $\Sigma'(p)$  is defined as  $\Sigma'(p) \equiv \Sigma(p) - \Delta\Sigma(p)\sigma_+$ , where the non-analytic term is absent.

With respect to the  $\omega$ -dependence, we have  $\partial_{\omega}\Sigma'(0) = \sigma_3$ . Because of a symmetry relation  $\Sigma_{12}(p) = \Sigma_{12}(-p)$ , we find that the off-diagonal element satisfies  $\partial_{\omega}\Sigma'_{12}(0) = 0$ . For  $\partial_{\omega}\Sigma'_{11}(0)$ , we have an identity [9, 49]

$$\partial_{\omega}\Sigma'_{11}(0) = \frac{\partial^2\Omega'}{\partial\mu\partial n_0} = 1. \quad (59)$$

In the last equality, we have employed the relation (B4) in the isothermal condition shown in Appendix B. The first equality indicates that the differential  $\partial_{\omega}$  is related to  $\partial_{\mu}$ , since the self-energy is constructed from the non-interacting Green's function  $G^{(0)}(p) = 1/(\omega - \varepsilon_{\mathbf{p}} + \mu)$  and then the infinitesimally small increase of the energy  $\omega + \delta\omega$  in the self-energy  $\Sigma$  is regarded as the infinitesimally small increase of the chemical potential  $\mu + \delta\omega$  in a Green's function  $G^{(0)}$  that constructs  $\Sigma$  [9]. With respect to the second order of  $\mathbf{p}$  or  $\omega$ , similar relations are obtained, giving the forms [9]

$$\partial_{\omega}^2\Sigma'(0)|-\rangle = \frac{1}{n_0} \frac{\partial^2\Omega'}{\partial\mu^2}|-\rangle = -\frac{n}{n_0 m c_T^2}|-\rangle, \quad (60)$$

$$\partial_{\mathbf{p}}^2\Sigma'(0)|-\rangle = \frac{n'}{m n_0}|-\rangle, \quad (61)$$

where  $c_T$  is the isothermal sound speed (See Appendix B). Note that although the relations between the vertex functions hold at nonzero temperatures because the diagrammatic structure is the same as in the case at  $T = 0$ , the relations between the thermodynamic quantities and the differentiations of vertex functions with respect to  $\omega$  and  $p_i$  shown here do not hold at nonzero temperatures.

The single-particle Green's function in the low-energy regime is reduced into [36] (See Appendix C)

$$G(p) \simeq \frac{n_0 m c_T^2}{n} \frac{1}{\omega^2 - c_T^2 \mathbf{p}^2} \begin{pmatrix} 1 & -1 \\ -1 & 1 \end{pmatrix} - \frac{1}{4\Sigma_{12}(p)} \begin{pmatrix} 1 & 1 \\ 1 & 1 \end{pmatrix}. \quad (62)$$

The first term in (62) is the leading term of  $G$ , which provides the phonon spectrum of the single-particle excitation, whose sound speed  $c_T$  corresponds to the isothermal sound speed related to the compressibility (B9). This first term is important to the low-energy behavior of the density and current correlation functions, and essential for the transverse susceptibility  $G_\perp(p) = -\langle -|G(p)|- \rangle/4$  with respect to the BEC order parameter [38, 45]. The second term in (62) also provides the infrared divergence, because of the Nepomnyashchii-Nepomnyashchii identity, where the infrared divergence of the second term is much weaker than that of the first term in (62). This weak infrared divergent second term never plays an essential role in the density and current correlation functions. However, it plays an important role in the longitudinal susceptibility  $G_\parallel(p) = -\langle +|G(p)|+ \rangle/4$  [38, 43–45, 47, 50]. The transverse and longitudinal fluctuation operators are not commutable [44, 45]. Since the transverse fluctuation is regarded as the phase fluctuation, the longitudinal fluctuation might be expected to represent the amplitude (Higgs) mode. However, the longitudinal susceptibility does not describe the gapped amplitude mode, and shows the weak infrared divergence in the low-energy limit, because it is provided from the convolution of the phase-phase correlation function. The response function that can capture the Higgs mode is the scalar susceptibility [51].

In the low-energy regime, the density and current correlation functions (30) behave as [9]

$$\chi_{00}(p) \simeq \frac{n}{m} \frac{\mathbf{p}^2}{\omega^2 - c_T^2 \mathbf{p}^2}, \quad (63)$$

$$\chi_{0i}(p) \simeq \chi_{i0}(p) \simeq \frac{n}{m} \frac{\omega p_i}{\omega^2 - c_T^2 \mathbf{p}^2}, \quad (64)$$

$$\chi_{ij}(p) \simeq \frac{nc_T^2}{m} \frac{p_i p_j}{\omega^2 - c_T^2 \mathbf{p}^2}. \quad (65)$$

Here,  $c_T$  is the isothermal sound speed that can be found in the single-particle Green's function (62). As summarized in Appendix D, the 1PI part  $\chi_{\mu\nu}^{1\text{PI}}(q)$  can be given by [9]

$$\chi_{00}^{1\text{PI}}(0) = \frac{1}{2} T \frac{\partial}{\partial \mu} \sum_p \text{Tr}[G(p)] = -\frac{\partial n'}{\partial \mu}, \quad (66)$$

$$\chi_{i0}^{1\text{PI}}(0) = \frac{1}{2} T \sum_p \frac{p_i}{m} \frac{\partial}{\partial \mu} \text{Tr}[\sigma_3 G(p)] = 0, \quad (67)$$

$$\chi_{0j}^{1\text{PI}}(0) = -\frac{1}{2} T \sum_p \frac{\delta}{\delta q_j} \text{Tr}[G(p)] = 0, \quad (68)$$

$$\chi_{ij}^{1\text{PI}}(0) = -\frac{1}{2} T \sum_p \frac{p_i}{m} \frac{\delta}{\delta q_j} \text{Tr}[\sigma_3 G(p)] = 0. \quad (69)$$



The density-density correlation function remains nonzero in the low-energy and low-momentum limit. On the other hand, the density-current and current-current correlation functions vanish in the same limit.

Using (57), we have the following simple expression of the density and current vertex in the low-energy and low-momentum limits:

$$\Upsilon_\nu(p) \simeq \begin{cases} \frac{\omega}{2\sqrt{n_0}} \frac{\partial n'}{\partial \mu} |-\rangle & (\nu = 0) \\ \frac{p_i}{2\sqrt{n_0}} \frac{n}{m} |-\rangle & (\nu = i = 1, 2, 3). \end{cases} \quad (70)$$

The density and current vertex vanishes in the static and low-momentum limits, i.e.,  $\Upsilon_\nu(0) = 0$ , which is consistent with the exact identity (45). To obtain (70), we employed the identity (B4) in the isothermal condition for  $\nu = 0$ , which is the consequence of the Nepomnyashchii–Nepomnyashchii identity, and employed the relation  $\sum_{\mathbf{p}} p_i \partial n_{\mathbf{p}} / \partial p_j = -\delta_{ij} n'$  for  $\nu = i = 1, 2, 3$ , where  $n_{\mathbf{p}}$  is the Bose distribution function.

The 1PR parts of correlation functions are then of the forms

$$\chi_{00}^{1\text{PR}}(p) = \frac{1}{n_0} \left( \frac{\omega}{2} \frac{\partial n'}{\partial \mu} \right)^2 \langle -|G(p)|-\rangle, \quad (71)$$

$$\chi_{0i}^{1\text{PR}}(p) = \chi_{i0}^{1\text{PR}}(p) = \frac{n\omega p_i}{4mn_0} \frac{\partial n'}{\partial \mu} \langle -|G(p)|-\rangle, \quad (72)$$

$$\chi_{ij}^{1\text{PR}}(p) = \frac{n^2}{n_0} \frac{p_i}{2m} \frac{p_j}{2m} \langle -|G(p)|-\rangle, \quad (73)$$

which provide

$$\chi_{00}^{1\text{PR}}(p) \simeq \frac{n}{m} \frac{\mathbf{p}^2}{\omega^2 - c_{\text{T}}^2 \mathbf{p}^2} + \frac{\partial n'}{\partial \mu}, \quad (74)$$

$$\chi_{i0}^{1\text{PR}}(p) \simeq \chi_{0i}^{1\text{PR}}(p) \simeq \frac{n}{m} \frac{\omega p_i}{\omega^2 - c_{\text{T}}^2 \mathbf{p}^2}, \quad (75)$$

$$\chi_{ij}^{1\text{PR}}(p) \simeq \frac{nc_{\text{T}}^2}{m} \frac{p_i p_j}{\omega^2 - c_{\text{T}}^2 \mathbf{p}^2}. \quad (76)$$

Here, we used a relation

$$\langle -|G(p)|-\rangle = \frac{4n_0 m c_{\text{T}}^2}{n} \frac{1}{\omega^2 - c_{\text{T}}^2 \mathbf{p}^2}, \quad (77)$$

which is conveniently obtained from (62). From Eqs. (62) and (77), the effect of the Nepomnyashchii–Nepomnyashchii identity and the infrared divergence of the longitudinal susceptibility  $G_{\parallel} = -\langle +|G|+\rangle/4 = 1/4\Sigma_{12}(0)$ , which comes from the second term of (62),

are found to be irrelevant to the density and current correlation functions. The correlation functions (63)-(65) can be obtained from the 1PI parts (66)-(69) and the 1PR parts (74)-(76).

The density-density correlation functions (63) satisfies the compressibility zero-frequency sum-rule, giving the form [5, 40]

$$\lim_{\mathbf{p} \rightarrow 0} \chi_{00}(0, \mathbf{p}) = -\frac{n}{mc_T^2}. \quad (78)$$

The compressibility zero-frequency sum-rule is exhausted by the 1PI part. In the low-energy limit, the 1PI and 1PR parts of the density-density correlation function in (66) and (74) behave as

$$\lim_{\mathbf{p} \rightarrow 0} \chi_{00}^{1\text{PI}}(0, \mathbf{p}) = -\frac{n}{mc_T^2}, \quad \lim_{\mathbf{p} \rightarrow 0} \chi_{00}^{1\text{PR}}(0, \mathbf{p}) = 0. \quad (79)$$

The 1PR part vanishes in the static and low-momentum limits, and does not contribute to the compressibility zero-frequency sum-rule.

The leading term of the single-particle Green's function (62) and the density and current correlation functions (63)-(65) share the pole, which provides the phonon excitations. Because of the presence of the BEC, the two-particle Green's function involves the single-particle Green's function as in the 1PR part (16). This contribution directly involves the single-particle property to the density correlation function. Since the self-energy in the single-particle Green's function can be related to thermodynamic quantities as discussed in this section, which can provides the phonon dispersion relation with the isothermal sound speed, the density correlation function can consistently describe the sound mode, the speed of which is defined in terms of the macroscopic compressibility. The paper by Huang and Klein [49] also provides a useful discussion about the phonon mode in BEC.

The single-particle excitation is also related to the superfluidity. An interesting relation between them owes to the Josephson sum-rule [6, 7], given by

$$\rho_s = -\lim_{\mathbf{p} \rightarrow 0} \frac{m^2 n_0}{\mathbf{p}^2 G_{11}(0, \mathbf{p})}, \quad (80)$$

where  $\rho_s$  is the superfluid mass density. By using Eq. (62) as well as the relation  $\Delta\Sigma(p) \gg \mathbf{p}^2$  in the small momentum regime, we find the relation

$$\rho_s = mn, \quad (81)$$

which indicates that the superfluid mass density is exactly the total mass density at  $T = 0$ .

The current-current response function can be decomposed into the longitudinal and transverse response functions, given by [8, 10, 150]

$$\chi_{ij}(p) = \frac{p_i p_j}{\mathbf{p}^2} \chi_L(p) + \left( \delta_{ij} - \frac{p_i p_j}{\mathbf{p}^2} \right) \chi_T(p). \quad (82)$$

These longitudinal and transverse response functions are extracted from the relations [8]

$$\chi_L(p) = \sum_{i,j} \frac{p_i p_j}{\mathbf{p}^2} \chi_{ij}(p), \quad (83)$$

$$\chi_T(p) = \frac{1}{2} \sum_{i,j} \left( \delta_{i,j} - \frac{p_i p_j}{\mathbf{p}^2} \right) \chi_{ij}(p). \quad (84)$$

The longitudinal response function satisfies the  $f$ -sum rule  $\chi_L(\mathbf{p} \rightarrow 0, 0) = -n/m$  and the transverse response function provides the normal fluid density  $n_n$ , given by  $\chi_T(\mathbf{p} \rightarrow 0, 0) = -n_n/m$  [3, 8, 10, 150]. As a result, the superfluid mass density can be given by  $\rho_s = m^2 \lim_{\mathbf{p} \rightarrow 0} [\chi_T(\mathbf{p}, 0) - \chi_L(\mathbf{p}, 0)]$ . Using the results (69) and (73), we obtain

$$\lim_{\mathbf{p} \rightarrow 0} \chi_L(\mathbf{p}, 0) = \lim_{\mathbf{p} \rightarrow 0} \frac{n^2}{n_0} \frac{\mathbf{p}^2}{(2m)^2} \langle -|G(\mathbf{p}, 0)|- \rangle = -\frac{n}{m}, \quad (85)$$

$$\lim_{\mathbf{p} \rightarrow 0} \chi_T(\mathbf{p}, 0) = 0, \quad (86)$$

which is consistent with the  $f$ -sum rule as well as with the fact that at  $T = 0$ , the normal fluid density is absent and the superfluid mass density is equal to the total mass density as in Eq. (81).

## V. EXPERIMENTAL AND THEORETICAL STUDIES OF SOUND MODES IN SUPERFLUID

This section presents an overview of the experimental and theoretical studies of excitations in superfluid  $^4\text{He}$  and in BECs of ultracold atomic gases, which will be helpful to bridge both fields and to push further the study of the single-particle and collective excitations in BECs in ultracold atoms.

The static structure and dynamic structure have been intensively and extensively studied on the superfluid liquid  $^4\text{He}$  experimentally [52–58]. The dynamic structure factor  $S(\mathbf{q}, \omega)$  consists of a sharp peak superimposed on a broad background in the superfluid  $^4\text{He}$  [52, 55–57, 61–67]. The sharp peak in  $S(\mathbf{q}, \omega)$  is interpreted as a collective density mode as well

as a (single)-quasiparticle excitation arising from the 1PR part of the density response function  $\chi_{00}^{1PR}$  [56, 57, 65, 66], where the density and single-particle responses have the same pole [57, 66, 68]. The broad component is interpreted as the multi-particle excitation originated from the 1PI part of the density response function  $\chi_{00}^{1PI}$  [57, 62, 67].

The temperature dependence of  $S(\mathbf{q}, \omega)$  is quite different above and below  $T_c$  [56], and abruptly changes at  $T_c$  [57]. As the temperature increased, the sharp peak broadens [57, 65, 66], which is well described by quasiparticle-quasiparticle scattering [57], and it loses intensity [55–57, 65, 66], since the condensate density decreases, which includes the single-particle Green’s function to the density response function.

At low momentum regime, the superfluid has a single phonon mode [57, 65, 69], whose peak is very sharp at low  $T$ , where the phase-space for the decay of a single phonon into two is limited [56]. The sharp peak at the maxon momentum region is also interpreted as a contribution from a quasiparticle excitation [65]. In the high momentum regime, the superfluid  $^4\text{He}$  does not support a collective density mode [57], and the density response function in this momentum regime broadens in the normal and superfluid phases [57, 65, 70].

The broad component is considered as multi-quasiparticle excitations with the high-energy tail, which originates from roton-roton, maxon-maxon, and maxon-roton contributions [70, 71]. This broad continuum does not contain a collective mode in the superfluid phase [57], which starts from a finite positive energy [61]. The broad multiphonon component and high-frequency tail are largely temperature independent [56, 57, 72].

Above the critical temperature, the sharp peak phonon-maxon-roton excitation disappears from  $S(\mathbf{q}, \omega)$  [55–57, 65, 66], where the single-particle Green’s function does not contribute to the density response function [56]. In more detail, the sharp component disappears in the maxon and roton momentum regions, but the peak remains well defined in the low-momentum phonon region, which indicates the existence of a collective density mode [57, 65].

The dynamic structure factor  $S(\mathbf{q}, \omega)$  of the superfluid  $^4\text{He}$  has been also studied theoretically [57, 61, 65, 66, 70–83]. In the Bogoliubov approximation, the density-fluctuation excitation spectrum is identical to that of the quasiparticles. However, this approximation gives the incorrect relation  $\int_0^\infty S(\mathbf{q}, \omega) \omega d\omega = N_0 \mathbf{q}^2 / (2m)$ , where the correct sum-rule is proportional to  $N$  not to  $N_0$  [61]. Other approaches may be listed, such as the Hartree–Fock approximation and self-consistent Hartree approximation [74], the symmetric planer-spin model analysis explaining the light-scattering data [76], the formal expressions for the one-

and two-quasiparticle excitation [81], the two-roton bound states [83], and various sum-rules for the density and particle operators [84].

In the theoretical framework, it can be clearly seen that the condensate plays an essential role in coupling the density excitation and the quasiparticle excitation [57, 65, 66, 83–85], where this hybridization disappears above the critical temperature [83]. In the low momentum phonon regime, the single-particle Green’s function and density response function share the pole [9, 84]. Above the critical temperature, where the hybridization is absent, the maxon-roton peak vanishes in  $S(\mathbf{q}, \omega)$ , which suggests that the sharp maxon-roton intensity originates from the single-particle excitation and the BEC in the superfluid  $^4\text{He}$  [82].

For the hybridization, the dielectric formalism [66, 82, 86, 87] is an approach that fulfills the Ward identities related to the conservation of particle number and the breaking of the gauge symmetry, i.e., a conserving and gapless approach by using the continuity equation [87]. It gives the same pole in the single-particle Green’s function and the density correlation function in the superfluid phase [66, 87], and the density fluctuation is coupled into the single-particle excitation through the condensate [86].

The sound velocity [88–98] as well as the sound attenuation coefficient [89, 96, 99–105] are theoretically investigated, where theoretical approaches include the single-particle Green’s function approach [80, 88, 89, 94, 95], the collective description theory [90–92, 103, 106–110], and the kinetic equation approach [98, 99, 102, 111]. Since the single-particle Green’s function and density response function share the pole [84], the sound speed and damping are calculated from the pole of the single-particle Green’s function [80, 88, 89, 94, 95]. The finite energy spread of phonon excitations are studied by using the thermodynamic perturbation theory assuming the possibility of the three-phonon interaction [88]. Using the Green’s function approach, the sound speed shows the temperature dependence given in the increase as  $T^4 \ln T$  [89, 94, 95] and the decrease as  $T^4$  [94, 95]; the damping rate shows the  $T^4$ -law [89, 94, 95], which comes from the three-phonon processes [89].

The collective description is a theory described by the canonical collective variables, i.e., the density fluctuation and velocity operators [90–92, 103, 106–110], which is a divergent free approach [90–92]. The collective description is employed to study energy spectrum [90–92, 109], focusing on effects of the phonon-phonon interaction [90], and phonon-roton interaction [92], which play an important role in the phonon velocity and roton minimum, and is employed to study the temperature dependence of the sound velocity and the absorption

coefficient including the thermal roton effect [103].

The kinetic equation is also applied to study the sound velocity and absorption [98, 99, 102, 111]. In this approach, collisions between excitations are assumed to be not frequent in the superfluid helium at low temperatures, and thus the kinetic equation in the collisionless regime is employed. The sound velocity in the sufficiently low temperatures increases as  $T^4 \ln(\text{const.}/T)$  [99], where the constant is very small [102], and the absorption is reported to follow the  $T^6$ -law [99].

Since successful creation of the BEC in alkali atom gases [128, 129], the condensate excitation in ultracold gases has been intensively and extensively studied [15, 16, 130]. Sudden modification of the trapping potential can create the local density fluctuation, and the dynamical propagation of the density fluctuation has been measured by using the phase-contrast images, where the propagation speed is consistent with the Bogoliubov theory [20]. Two-photon Bragg scattering is a useful tool to study the excitation in the BEC of ultracold gases [21]. The Bragg spectroscopy has been applied to measure the structure factor of the BEC in the phonon regime, the line shift and line strength of which are consistent with the results of the local density approximation [22]. The Bragg pulses have also been applied to observe the Bogoliubov transformation for a BEC [131, 132], and to reveal the wide range of the excitation spectrum from the phonon regime to the single-particle regime, which is also consistent with the Bogoliubov theory with the local density approximation [23]. By using the Bragg spectroscopy, experiments have probed the excitation in a strongly interacting BEC [24], as well as the roton-type excitation in BECs with cavity-mediated long-range interactions [133], with spin-orbit couplings [134], in shaken optical lattices [135], and with dipole interactions [136]. Recently, the sound propagation of the BEC trapped in a box trap has been intensively and extensively studied, including a uniform two-dimensional Bose gas [137], and a cylindrical box trap with tuning the atomic density [138], which are free from the conventional restriction of the harmonic trap potential.

Through the development of the study on BECs in ultracold atoms, theories have been proposed [27–30] that cast doubt upon the conventional wisdom about the BEC, where those recent theories claim that the dispersion relation of the single-particle excitation is not equal to that of the collective excitation in the low-energy and low-momentum regime, which contradicts the earlier result given by Gavoret and Nozières [9]. It is concluded from two different approaches: the Luttinger-Ward thermodynamic functional approach ( $\Phi$ -derivable

approximation) [27–29, 139] and a functional renormalization group approach [30, 140].

The Luttinger-Ward thermodynamic functional approach [27–29, 139] is useful for considering the theory satisfying the Noether’s theorem and the Goldstone’s theorem, which may cure the so-called conserving-gapless dilemma [141–144]. The papers [28, 29] are concluded that the self-energy contribution should be one-particle reducible (1PR), because the 1PR contribution cures the conserving-gapless dilemma. As a result, the two-particles Green’s function has the pole showing the collective sound mode; on the other hand, the single-particle Green’s function provides a bubbling mode with a considerable decay rate rather than the sound mode, which results in no well-defined quasiparticle in BECs [28]. However, in general, in the case where the self-energy contribution is included to the Green’s function through the Dyson-Beliaev equation, the one-particle irreducible part should be employed. Otherwise, multi-counting of diagrammatic contribution emerges in the full Green’s function. In this regard, even if the 1PR approximation may avoid the conserving-gapless dilemma, it provides a problem, namely, the trilemma among conserving, gapless and 1PR approximation in the BEC theory.

By using the exact renormalization-group technique [145, 146], the study [30] concluded that the one-particle density matrix approaches the condensate density as  $1/r^{d-2+\eta}$  asymptotically with an anomalous dimension  $\eta > 0$ , which gives the single-particle Green’s function  $G_{11} \propto 1/\mathbf{p}^{2-\eta}$  in the low-momentum regime. As a result, the paper [30] claimed that a three-dimensional BEC at  $T = 0$  does not have the Bogoliubov phonon mode. The behavior  $G_{11} \propto 1/\mathbf{p}^{2-\eta}$ , however, provides an unphysical situation, which gives the superfluid density  $\rho_s$  being infinity according to the Josephson sum-rule (80) [6–8]. The anomalous dimension  $\eta > 0$  also violates the Bogoliubov operator inequality  $-G_{11}(0, \mathbf{p}) \geq mn_0/(n\mathbf{p}^2)$  [8, 10, 143, 147–150]. According to this Bogoliubov operator inequality, the relation  $\eta = 0$  should hold for  $T < T_c$  [148]. The possibility of the anomalous dimension  $\eta > 0$  emerges only in the case at precisely  $T_c$ , where the correlation length diverges [148].

Other approach, the extension of Bijl–Feynman formula, also provides the result that the energy spectrum of the single-particle excitation is distinct from that of the collective excitation, and the lifetime of the quasiparticles remains finite even in the long-wavelength limit [31]. In this respect, the Josephson sum-rule (80) and the Bogoliubov operator inequality [143, 147–150] could be useful criteria for the result contradictory to the conventional wisdom about the single-particle excitation and the collective excitation in BECs.

## VI. DENSITY RESPONSE FUNCTION IN RANDOM PHASE APPROXIMATION

The matrix formalism is a useful tool to develop many-body theories, such as the random phase approximation (RPA), for studying many-body effects as well as the density-density correlation function in BECs. The same idea of the matrix formalism for the BEC may be found in the study of an effective roton-maxon interaction in liquid He II [151]. In the BEC phase, the density-density correlation function is constructed from the sum of the 1PI and 1PR parts as in (30), i.e.,  $\chi_{00} = \chi_{00}^{1\text{PI}} + \chi_{00}^{1\text{PR}}$ . In the following, we omit the subscript describing the density vertex  $\mu = \nu = 0$  in the polarization function  $\chi$  as well as the density vertices  $\Upsilon$  and  $\Upsilon^\dagger$ , for simplicity.

We consider the 2PI parts  $I(p, p'; q)$ ,  $J(p; q)$  and  $J^\dagger(p; q)$  introduced in Sec. II as the simplest contributions, given by

$$I(p, p'; q) = U + \frac{1}{2} |f_0\rangle U \langle f_0| \equiv \hat{U}, \quad (87)$$

$$J(p, q) = -\sqrt{-1} \hat{U} (\mathcal{G}_{1/2} + \hat{T} \mathcal{G}_{1/2}), \quad (88)$$

$$J^\dagger(p, q) = -\sqrt{-1} (\mathcal{G}_{1/2}^\dagger + \mathcal{G}_{1/2}^\dagger \hat{T}) \hat{U}, \quad (89)$$

where the first and second terms in  $\hat{U}$  provide the Hatree and Fock contributions in the present matrix formalism, respectively. By assuming the momentum and frequency-dependence of the four and three point vertices as  $\Gamma(p, p'; q) = \Gamma(q)$ ,  $P(p; q) = P(q)$ , and  $P^\dagger(p; q) = P^\dagger(q)$ , we construct the random phase approximation by using Eqs. (18), (22) and (23), giving the forms

$$\Gamma(q) = \frac{1}{1 - \hat{U} \Pi(q)} \hat{U}, \quad (90)$$

$$P(q) = -\sqrt{-1} \Gamma(q) (1 + \hat{T}) \mathcal{G}_{1/2}, \quad (91)$$

$$P^\dagger(q) = -\sqrt{-1} \mathcal{G}_{1/2}^\dagger (1 + \hat{T}) \Gamma(q), \quad (92)$$

where  $\Pi(q) = -T \sum_p K_0(p; q)$ . The 1PI part of the density correlation functions and the



density vertices are also given by

$$\chi^{\text{IPI}}(q) = \frac{1}{2} \langle f_0 | [\Pi(q) + \Pi(q)\Gamma(q)\Pi(q)] | f_0 \rangle, \quad (93)$$

$$\Upsilon(q) = -\sqrt{-1} \left[ G_{1/2} + \frac{1}{2} \mathcal{G}_{1/2}^\dagger (1 + \hat{T}) \Gamma(q) \Pi(q) | f_0 \rangle \right], \quad (94)$$

$$\Upsilon^\dagger(q) = -\sqrt{-1} \left[ G_{1/2}^\dagger + \frac{1}{2} \langle f_0 | \Pi(q) \Gamma(q) (1 + \hat{T}) \mathcal{G}_{1/2} \right]. \quad (95)$$

We take the following bare part of the two-particle Green's function

$$K_0(p; q) = g(p + q) \otimes g(-p), \quad (96)$$

where  $g(p)$  is the single-particle Green's function, given by

$$g(p) = \begin{cases} \frac{1}{i\omega_n \sigma_3 - \xi_{\mathbf{p}} - U n_0 \sigma_1} & (T \leq T_c) \\ \frac{1}{i\omega_n \sigma_3 - \varepsilon_{\mathbf{p}} + \mu - \Sigma_{11}(0)} & (T \geq T_c), \end{cases} \quad (97)$$

where  $\xi_{\mathbf{p}} = \varepsilon_{\mathbf{p}} + U n_0$ . At  $T \leq T_c$ , we employed the Hartree–Fock–Bogoliubov–Popov (Shohno) approximation [46, 142, 152–155]. At  $T \geq T_c$ , the effective chemical potential is taken to be  $\mu - \Sigma_{11}(0)$ , since the Green's function  $g$  has a pole of a gapless dispersion law at the critical temperature  $T_c$ , with satisfying the Hugenholtz-Pines relation  $\mu = \Sigma_{11}(0)$ . The polarization function has a relation

$$\Pi(q) = \begin{pmatrix} \Pi_{11}(q) & \Pi_{12}(q) & \Pi_{12}(q) & \Pi_{14}(q) \\ \Pi_{12}(q) & \Pi_{22}(q) & \Pi_{14}(q) & \Pi_{12}^*(q) \\ \Pi_{12}(q) & \Pi_{14}(q) & \Pi_{22}(q) & \Pi_{12}^*(q) \\ \Pi_{14}(q) & \Pi_{12}^*(q) & \Pi_{12}^*(q) & \Pi_{11}^*(q) \end{pmatrix}, \quad (98)$$

which originates from the symmetry relations  $g_{22}(p) = g_{11}(-p)$  as well as  $g_{12}(p) = g_{12}(-p)$ . (The detailed expressions of  $\Pi_{11,12,14,22}$  are summarized in Appendix E.)

The four point vertex in this approximation can be conveniently decomposed into the  $T$ -matrix  $\mathcal{T}(q)$  given by the ladder type diagrams and the effective interaction  $U_{\text{eff}}(q)$  including the density fluctuation, given by

$$\begin{aligned} \Gamma(q) = & \mathcal{T}(q) + \frac{1}{2} |f_0\rangle U_{\text{eff}}(q) \langle f_0| + \frac{1}{2} \gamma(q) U_{\text{eff}}(q) \gamma^\dagger(q) \\ & + \frac{1}{2} \gamma(q) U_{\text{eff}}(q) \langle f_0| + \frac{1}{2} |f_0\rangle U_{\text{eff}}(q) \gamma^\dagger(q), \end{aligned} \quad (99)$$

where

$$\mathcal{T}(q) = \frac{U}{1 - U\Pi(q)}, \quad (100)$$

$$U_{\text{eff}}(q) = \frac{U}{1 - U\chi_{\text{R}}(q)}, \quad (101)$$

and  $\gamma(q) = \mathcal{T}(q)\Pi(q)|f_0\rangle$  and  $\gamma^\dagger(q) = \langle f_0|\Pi(q)\mathcal{T}(q)$ . Here,  $\chi_{\text{R}}(q)$  is the regular part of the density-density correlation function including the vertex correction, giving the form

$$\chi_{\text{R}}(q) = \frac{1}{2}\langle f_0|[\Pi(q) + \Pi(q)\mathcal{T}(q)\Pi(q)]|f_0\rangle, \quad (102)$$

which also give the 1PI part of the density correlation function

$$\chi^{\text{1PI}}(q) = \frac{\chi_{\text{R}}(q)}{1 - U\chi_{\text{R}}(q)}. \quad (103)$$

The density vertices  $\Upsilon$  and  $\Upsilon^\dagger$  are then given by

$$\Upsilon(q) = -\sqrt{-1} \left[ G_{1/2} + \frac{1}{2}\mathcal{G}_{1/2}^\dagger(1 + \hat{T})\gamma(q) \right] A(q), \quad (104)$$

$$\Upsilon^\dagger(q) = -\sqrt{-1}A(q) \left[ G_{1/2}^\dagger + \frac{1}{2}\gamma^\dagger(q)(1 + \hat{T})\mathcal{G}_{1/2} \right], \quad (105)$$

where  $A(q) = [1 + U_{\text{eff}}(q)\chi_{\text{R}}(q)]$ . Note that because of the relation (98), five elements  $\mathcal{T}_{11,12,14,22,23}$  are needed to construct the  $T$ -matrix  $\mathcal{T}$ , which is given by

$$\mathcal{T}(q) = \begin{pmatrix} \mathcal{T}_{11}(q) & \mathcal{T}_{12}(q) & \mathcal{T}_{12}(q) & \mathcal{T}_{14}(q) \\ \mathcal{T}_{12}(q) & \mathcal{T}_{22}(q) & \mathcal{T}_{23}(q) & \mathcal{T}_{12}^*(q) \\ \mathcal{T}_{12}(q) & \mathcal{T}_{23}(q) & \mathcal{T}_{22}(q) & \mathcal{T}_{12}^*(q) \\ \mathcal{T}_{14}(q) & \mathcal{T}_{12}^*(q) & \mathcal{T}_{12}^*(q) & \mathcal{T}_{11}(q) \end{pmatrix}. \quad (106)$$

Above the critical temperature, the 1PI part of the density-density correlation function is given by

$$\chi^{\text{1PI}}(q) = \frac{\Pi_{22}(q)}{1 - 2U\Pi_{22}(q)}, \quad (107)$$

because we have  $g_{12}(p) = \Pi_{12,14}(p) = 0$  at  $T \geq T_c$ . At the same temperature regime, the regular part is given by

$$\chi_{\text{R}}(q) = \frac{\Pi_{22}(q)}{1 - U\Pi_{22}(q)}. \quad (108)$$

The  $T$ -matrix  $\mathcal{T}$  at  $T \geq T_c$  has a diagonal form, whose matrix elements are given by

$$\mathcal{T}_{11(22)}(q) = \frac{U}{1 - U\Pi_{11(22)}(q)}. \quad (109)$$

For the single-particle Green's function  $G(p)$ , we include many-body effects to the self-energy by using the RPA for focusing on density fluctuations, which is given by

$$\begin{aligned} \Sigma_{11}(p) = & (n_0 + \tilde{n})U_{\text{eff}}(0) \\ & + n_0 U_{\text{eff}}(p) - T \sum_q U_{\text{eff}}(q) g_{11}(p - q), \end{aligned} \quad (110)$$

$$\Sigma_{12}(p) = n_0 U_{\text{eff}}(p), \quad (111)$$

where  $\tilde{n} = -T \sum_p g_{11}(p)$ .

The density vertex  $\Upsilon$  in the RPA given in (104) does not satisfy the zero-frequency density vertex identity  $\Upsilon(0) = 0$ . In the static and low-momentum limit, the density vertices given in (104) and (105) are reduced to

$$\begin{pmatrix} \Upsilon(0) \\ \Upsilon^\dagger(0) \end{pmatrix} = \frac{\sqrt{n_0}}{1 - U\chi_R(0)} \frac{2\Gamma'(0)}{U} \begin{pmatrix} |+\rangle \\ \langle +| \end{pmatrix} \quad (112)$$

where

$$\chi_R(0) = -\frac{1}{U} \frac{1 - U\Pi'(0)}{2 - U\Pi'(0)}, \quad \Gamma'(0) = \frac{U}{2 - U\Pi'(0)}, \quad (113)$$

with

$$\Pi'(q) = \Pi_{11}(q) + \Pi_{22}(q) + 2\Pi_{14}(q) + 4\Pi_{12}(q). \quad (114)$$

Each polarization function  $\Pi_{ij}$  exhibits an infrared divergence. For example, in the three dimensional system at  $T \neq 0$ , the polarization functions exhibit the infrared divergence, giving the form  $\Pi_{11,12,22,14}(\mathbf{p}, 0) \propto 1/|\mathbf{p}|$  at small  $\mathbf{p}$  [38]. Because of a relation  $g_{11}(p) = -g_{12}(p)$  in the low-energy limit, the following exact relation holds:

$$\lim_{\mathbf{p} \rightarrow 0} \Pi_{11,22,14}(i\omega_n = 0, \mathbf{p}) = -\lim_{p \rightarrow 0} \Pi_{12}(i\omega_n = 0, \mathbf{p}). \quad (115)$$

All the infrared divergences are thus canceled out each other in  $\Pi'$ , and then the function  $\Pi'(0)$  converges at  $T < T_c$ . By using (E1), (E2), (E3) as well as (E4), we have its explicit form given by

$$\lim_{\mathbf{q} \rightarrow 0} \Pi'(0, \mathbf{q}) = \sum_{\mathbf{p}} \frac{\varepsilon_{\mathbf{p}}^2}{E_{\mathbf{p}}^2} \left( \frac{\partial n_{\mathbf{p}}}{\partial E_{\mathbf{p}}} - \frac{1 + 2n_{\mathbf{p}}}{2E_{\mathbf{p}}} \right), \quad (116)$$

where  $n_{\mathbf{p}}$  is the Bose-distribution function  $n_{\mathbf{p}} = 1/(e^{E_{\mathbf{p}}/T} - 1)$  with  $E_{\mathbf{p}} = \sqrt{\varepsilon_{\mathbf{p}}(\varepsilon_{\mathbf{p}} + 2Un_0)}$ . At  $T < T_c$ , therefore, the density vertex parts in (112) provide  $\Upsilon(0) \neq 0$ .

This problem may be avoided by adopting the simplified regular part of the density-density correlation function that does not include the vertex correction, giving the form

$$\chi_R^s(q) = \frac{1}{2} \langle f_0 | \Pi(q) | f_0 \rangle. \quad (117)$$

Using this simplified version, we may take a variant of the density vertices  $\Upsilon^s(q)$  and  $\Upsilon^{s\dagger}(q)$ , which are given by replacing  $A(q)$  in Eqs. (104) and (105) with  $A^s(q) = 1 + U_{\text{eff}}^s(q)\chi_R^s(q)$ , where

$$U_{\text{eff}}^s(q) = \frac{U}{1 - U\chi_R^s(q)}. \quad (118)$$

The simplified density vertex  $\Upsilon^s$  satisfies the identity  $\Upsilon^s(0) = 0$ . In the low-energy limit, this density vertex  $\Upsilon^s$  is reduced to

$$\begin{pmatrix} \Upsilon^s(0) \\ \Upsilon^{s\dagger}(0) \end{pmatrix} = \frac{\sqrt{n_0}}{1 - U\chi_R^s(0)} \frac{2\Gamma'(0)}{U} \begin{pmatrix} |+\rangle \\ \langle +| \end{pmatrix}. \quad (119)$$

Since the simplified regular part is given by  $\chi_R^s(0) = \chi_{22}(0) + \chi_{14}(0)$ , which shows the infrared divergence, we thus obtain the density vertex that satisfies the zero-frequency density vertex identity  $\Upsilon(0) = 0$ .

According to the same reason, the off-diagonal self-energy (111) does not satisfy the Nepomnyashchii–Nepomnyashchii identity  $\Sigma_{12}(0) = 0$ . This problem is also avoided by replacing the effective interaction  $U_{\text{eff}}$  with  $U_{\text{eff}}^s$  in the off-diagonal self-energy (111), because the infrared divergence of  $\chi_R^s$  provides  $U_{\text{eff}}^s(0) = 0$ . As a result, the off-diagonal self-energy  $\Sigma_{12} = n_0 U_{\text{eff}}^s(p)$  is one of the candidates to satisfy the Nepomnyashchii–Nepomnyashchii identity [36, 37]. Other approaches that satisfies the Nepomnyashchii–Nepomnyashchii identity have been also discussed, including the description in terms of the hydrodynamic variables [38, 42, 46–48, 50, 156], the renormalization group approach [47, 48, 146, 157, 158], the large- $N$  expansion [47, 159] and the division approach into singular and nonsingular self-energies [38].

## VII. DENSITY AND SINGLE-PARTICLE SPECTRAL FUNCTION

This section serves as the study of the density response function and the single-particle spectral function in the BEC by using the formalism developed in the previous section. The

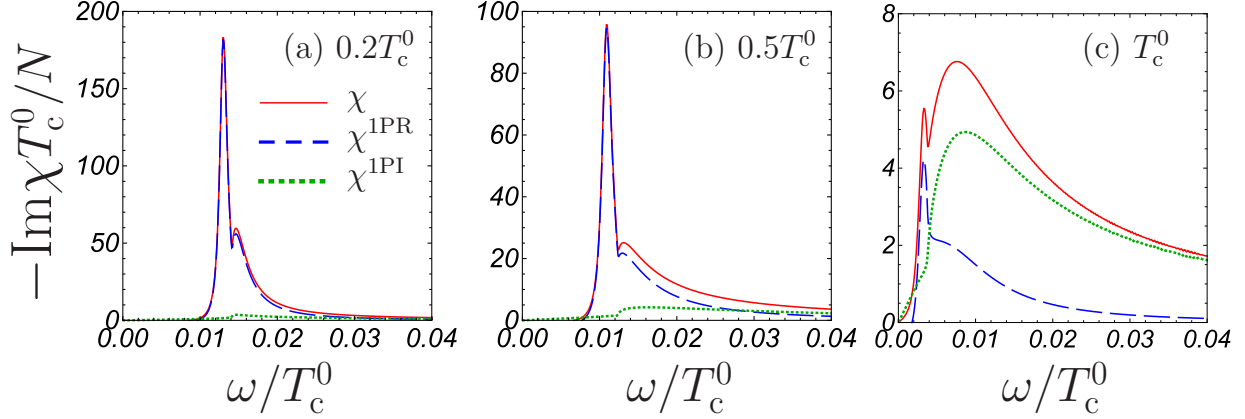


FIG. 5. Density response function at temperature (a)  $0.2T_c^0$ , (b)  $0.5T_c^0$ , and (c)  $T_c^0$ , where  $T_c^0$  is the critical temperature of an ideal Bose gas. We used the self-energies in (110) and (111), and the density vertex in (104) and (105), with the effective interaction (101) including the vertex correction. We also used the 1PI part in (103) also including the vertex correction. The critical temperature is given by  $T_c/T_c^0 \simeq 1 + 1.9an^{1/3}$  at the gas parameter  $an^{1/3} = 10^{-2}$ . We take the momentum  $q = 0.05q_0$ , where  $T_c^0 \equiv q_0^2/(2m)$ .

condensate density is calculated as a function of temperature, by solving the particle number equation with the non-condensate density (13), where below  $T_c$ , the chemical potential satisfies the Hugenholtz-Pines relation, and the self-energies are given in (110) and (111). We performed the analytic continuation based on Refs. [160, 161].

At the low temperature regime ( $0.2T_c^0$ ), where  $T_c^0$  is the critical temperature of an ideal Bose gas, the sharp peak emerges with the satellite structure in the density response function  $\chi$  (Fig. 5(a)). Since the 1PI part  $\chi^{1PI}$  is found to be negligibly small compared with the 1PR part  $\chi^{1PR}$ , the satellite peak is mainly originated from  $\chi^{1PR}$  part at the low temperature. This is stark contrast to the case of the multi-particle excitation in the superfluid  $^4\text{He}$ , which provides the significant broad peak. The multi-particle excitation in the superfluid  $^4\text{He}$  is originated from the roton-roton, maxon-maxon, and roton-maxon scattering and their bound states. Since the dispersion relation of the quasiparticle has extremum at the roton and maxon region, those provides the very large density of states owing to the van Hove singularity. This effect leads the pronounced contribution of the 1PI part to the density response function. In the present case without roton and maxon excitations, however, the satellite peak is originated from the 1PR part. For increasing temperature, the contribution

from the 1PI part is enhanced (Fig. 5(b)), and the density response function is mainly organized by the 1PI part close to  $T_c$  (Fig. 5(c)). Although the main structure of  $\chi$  in Fig. 5(c) is the broad peak with a tail in the high frequency side, one can see the small sharp peak structure at the low frequency side, which is originated from the 1PR part. Very close to the critical temperature, the 1PR part does not show the main contribution to the density response function, because the density vertex  $\Upsilon$  proportional to  $\sqrt{n_0}$  is small.

The temperature dependences of each contribution to  $\chi$  are summarized in Fig. 6. The density response function gives the striking sharp peak with the satellite structure, but at the intermediate temperature, the peak strength becomes weak and the satellite peak structure changes into the tail structure (Fig. 6(a)). The intensity of the density response function at the critical temperature is quite small compared with the case at the low temperature. The 1PR part shows the similar behavior to the total density response function  $\chi$ ; however, the 1PR part vanishes at the critical temperature (Fig. 6(b)). The 1PI part exhibits the striking sharp structure with a broad tail at  $0.1T_c^0$ ; on the other hand, as the temperature increase, this sharpness vanishes with the growth of the intensity (Fig. 6(c)). The spectral function of the single-particle excitation is also shown in Fig. 6(d). The structure of  $G_{11}$  in the low temperature regime provides the sharp peak with a small satellite peak, which is the same behavior as the density response functions  $\chi$  and  $\chi^{1PR}$ . However, at high temperature such as  $T_c^0$  and  $T_c$ , the satellite peak disappears, where the intensity of  $-\text{Im}G_{11}$  remains the same order as those in the low-temperature case, which is in contrast to the case for the density response function. In the density response function  $\chi$ , the peak of the 1PR part emergent from the single-particle excitation is suppressed by the density vertex  $\Upsilon$  proportional to  $\sqrt{n_0}$ .

In Figs. 5 and 6, we have discussed the structure of the density response function and the single-particle spectral function by using the self-energies (110) and (111) and the density vertex (104) and (105) both including the vertex correction. These qualitative features do not change in the case where the vertex correction is eliminated. Figure 7 shows the results with the density vertices  $\Upsilon^s$  and  $\Upsilon^{s\dagger}$  satisfying the identity  $\Upsilon^s(0) = 0$ , where the self-energy contribution is still given by (110) and (111). Figure 8 shows the results with the density vertex  $\Upsilon^s$  and  $\Upsilon^{s\dagger}$  as well as the self-energy contribution with the use of the effective interaction (118), which satisfies the Nepomnyashchii–Nepomnyashchii identity  $\Sigma_{12}(0) = 0$  [34]. Although the satellite peaks without the vertex correction in Figs. 7 and 8 are very

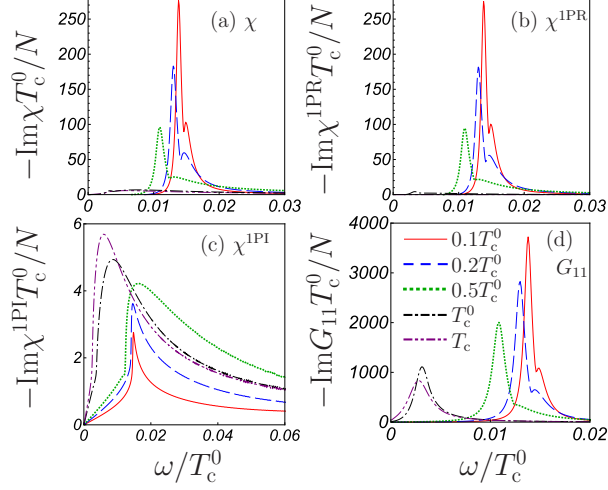


FIG. 6. Structure of the response functions at  $an^{1/3} = 10^{-2}$  and  $q = 0.05q_0$ . (a) The total density response function  $\chi$ , (b) the 1PR part  $\chi^{1PR}$ , (c) the 1PI part  $\chi^{1PI}$ , and (d) the single-particle Green's function  $G_{11}$ . We used the same Feynman diagrams as used in Fig. 5.

slightly enhanced compared with the result in Fig. 5, the qualitative features remain the same.

Above the critical temperature, the density response function is exhausted by the 1PI part, where the 1PR part is absent since  $\Upsilon = 0$ . By using the RPA, we found that the density response function at  $T > T_c$  has qualitatively the same structure at  $T = T_c$ , where a broad structure emerges and very long-lived collective excitations are absent. This is because the random phase approximation describes collisionless modes, and does not describe the hydrodynamic mode. In this sense, this result indicates that there is no long-lived collisionless sound modes in a normal Bose gas. The hydrodynamic analysis in the superfluid phase can be found in Ref. [141].

The origin of the satellite peak of the density response function can be discussed as follows: As shown in Figs. 5, 6, 7, and 8, the satellite peak of the density response function  $\chi$  is dominantly originated from the 1PR part  $\chi^{1PR}$  that includes the single-particle Green's function through the density vertex  $\Upsilon$ . We thus separately treat the self-energy contribution in the single-particle Green's function to discuss the origin of the satellite peaks [34]. The self-energy contribution in the BEC involves two-parts: diagonal and off-diagonal self-energies  $\Sigma_{11(12)}$ , which are also consists of two parts: condensate part  $\Sigma_{11(12),c}$  and non-condensate part  $\Sigma_{11(12),n}$ . For  $\Sigma_{12,n}$ , we consider the form  $\Sigma_{12,n}(p) = -\sum_q U_{\text{eff}}(p)g_{12}(p+q)$ . In order to

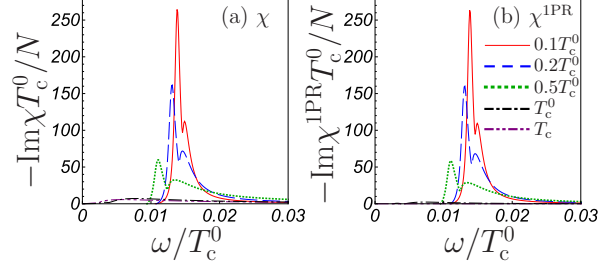


FIG. 7. Structure of the response functions at  $an^{1/3} = 10^{-2}$  and  $q = 0.05q_0$ . (a) The total density response function  $\chi$ , (b) the 1PR part  $\chi^{1PR}$ . We used the same structure of the self-energies and the 1PI part as in Fig. 5. For the density vertex, we employed  $\Upsilon^s$  and  $\Upsilon^{s\dagger}$ , which satisfies the zero-frequency density vertex identity  $\Upsilon^s(0) = 0$ .

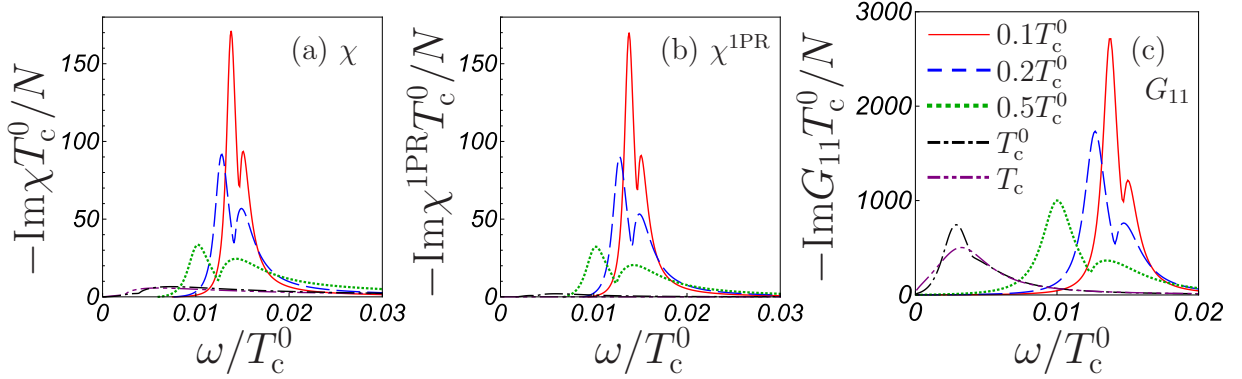


FIG. 8. Structure of the response functions at  $an^{1/3} = 10^{-2}$  and  $q = 0.05q_0$ . (a) The total density response function  $\chi$ , (b) the 1PR part  $\chi^{1PR}$ , and (c) the single-particle Green's function  $G_{11}$ . We used the self-energy satisfying the Nepomnyashchii–Nepomnyashchii identity  $\Sigma_{12}(0) = 0$ , where  $U_{\text{eff}}$  in (110) and (111) is replaced with  $U_{\text{eff}}^s$  in (118). For the density vertex, we employed  $\Upsilon^s$  and  $\Upsilon^{s\dagger}$ . We used the 1PI part in (103) including the vertex correction.

separately analyze each contribution, we first consider the Hartree–Fock–Bogoliubov type self-energies, which can include all the contributions  $\Sigma_{11(12),c}$ , and  $\Sigma_{11(12),n}$ , diagrammatically described in Fig. 9(b). In this approximation, the satellite peak can be seen (Fig. 9(a)), which is consistent with the case of the Hartree–Fock–Bogoliubov–Popov type self-energies that does not include  $\Sigma_{12,n}$ .

The emergent satellite peak is possibly originated from (i) the off-diagonal self-energy  $\Sigma_{12}$ ,



(ii) non-condensate part  $\Sigma_{11(12),n}$ , or (iii) condensate part  $\Sigma_{11(12),c}$ . Figure 9(a) shows the result of these contributions, where the self-energy contribution is selectively eliminated. The satellite peak still survives even if we eliminate the off-diagonal self-energy  $\Sigma_{12}$ , and the non-condensate part  $\Sigma_{11(12),n}$ . On the contrary, the satellite peak vanishes when the condensate part of the self-energy  $\Sigma_{11(12),c}$  is absent. In the Bogoliubov approximation, where we replace the effective interaction  $U_{\text{eff}}(p)$  with the bare interaction  $U$ , the satellite and the broadening of the sharp peak structure never emerge, which gives the Bogoliubov excitation showing the sharp peak of the quasiparticle with infinite life-time. The origin of the satellite peak is thus concluded as the many-body BEC effect, namely, the condensate part of the self-energy, which gives the interaction between the condensate and the quasiparticle in the background of the many-body density-fluctuated medium. The non-condensate part of the self-energies, showing the quasiparticle-quasiparticle interaction effect, is not important for the satellite peak, where the many-body effect of the density fluctuation is smeared out by quasiparticles with various momenta.

One of the feature of the excitation of a BEC at  $T = 0$  is that the correspondence of the spectrum between the single-particle excitation and the collective excitation in the low-energy regime [9]. We study the temperature dependence of these two excitations and discuss this correspondence by using the effective interaction including the vertex correction (Fig. 10). Except close to the critical temperature, the density spectral function is dominated by the 1PR part, and thus the peak position of  $\chi$  traces that of the 1PR part (Fig. 10(a)). The intensity of the 1PI part is weak and its structure is very broad compared with the 1PR part (Figs. 10(b) and (c)). The peak of the 1PI part is not monotonic function of the temperature, and close to  $T_c$ , the peak of  $\chi$  traces that of the 1PI part instead of the 1PR part, because the density vertex in the 1PR part becomes small. At the very low-temperature regime, we corroborated that the correspondence between the single-particle excitation peak and the collective excitation peak within the resolution of the numerical calculation. On the other hand, as the temperature increases, the peak of the single-particle excitation and that of the collective density excitation have a slight difference. This is due to the diminishing density vertex and the relatively increasing 1PI part as a function of the temperature.

We discuss the approximation dependence on the result of the correspondence of the spectrum between the single-particle excitation and the density collective excitation (Fig. 11).

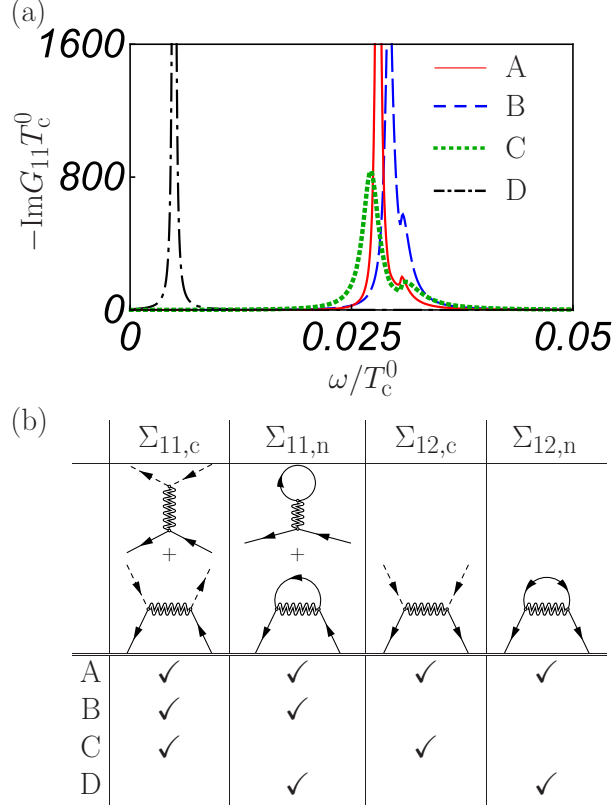


FIG. 9. Single-particle spectral function evaluated by various approximations. (a)  $G_{11}$  at  $T = 0.5T_c^0$  at  $an^{1/3} = 10^{-2}$  and  $q = 0.1q_0$ . (b) Feynman diagrams used in panel (a). The solid arrow represents the single-particle line, the dashed arrow the condensate line, and the wiggly line the effective interaction line  $U_{\text{eff}}$  including the vertex correction in (101).

In contrast to the case of Fig. 10, we employ the density vertex satisfying the identity  $\Upsilon^s(0) = 0$ , where the vertex correction is omitted. In this case, the temperature dependence of the peak position of  $\chi$  as well as  $\chi^{\text{1PR}}$  are quite different from the case in Fig. 10. As a result, the temperature dependence of the peak position may change, depending on approximations, such as the absence/existence of the vertex correction. However, in the very low temperature regime, we can still find the correspondence between the peak positions between the density response function and the single-particle Green's function.

The density response function and the single-particle spectral function are shown in the  $\omega$ - $q$  plane in Fig. 12. The peak of the single-particle excitation traces that of the density response function at low temperature ( $0.1T_c^0$ ). This correspondence cannot be seen at  $T_c$ , because of the absence of the BEC. At moderate temperature ( $0.5T_c^0$ ), although two peak po-

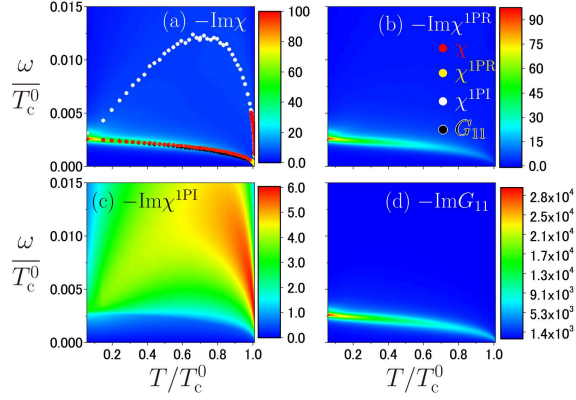


FIG. 10. Frequency and temperature dependence of the response functions. (a) The total density response function  $\chi$ , (b) the 1PR part  $\chi^{1PR}$ , (c) the 1PI part  $\chi^{1PI}$ , and (d) the single-particle Green's function  $G_{11}$ . Red, yellow, white, and black points represent the maximum peak positions of  $-\text{Im}\chi$ ,  $-\text{Im}\chi^{1PR}$ ,  $-\text{Im}\chi^{1PI}$ , and  $-\text{Im}G_{11}$ , respectively. We used the same self-energies, density vertex, effective interaction and the 1PI part as shown in Fig. 5.

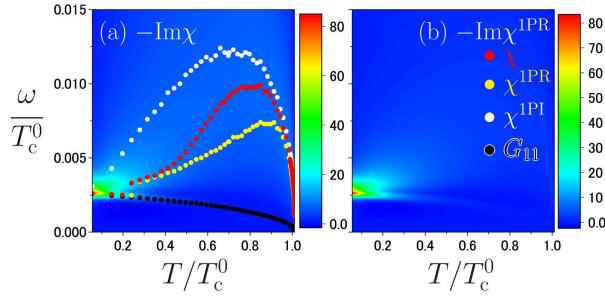


FIG. 11. Temperature and frequency dependence of the response functions. (a) The total density response function  $\chi$ , and (b) the 1PR part  $\chi^{1PR}$ . Red, yellow, white, and black points are the same as in Fig. 10. We used the same self-energies, effective interaction and the 1PI part as in Fig 10. For the density vertex, we employed  $\Upsilon^s$  and  $\Upsilon^{s\dagger}$ .

sitions are slightly different at high-momentum and high-energy regime, the correspondence may survives in the low-momentum and low-energy regime. At very low temperature, the peak position is well described by the Bogoliubov approximation, although the satellite peak

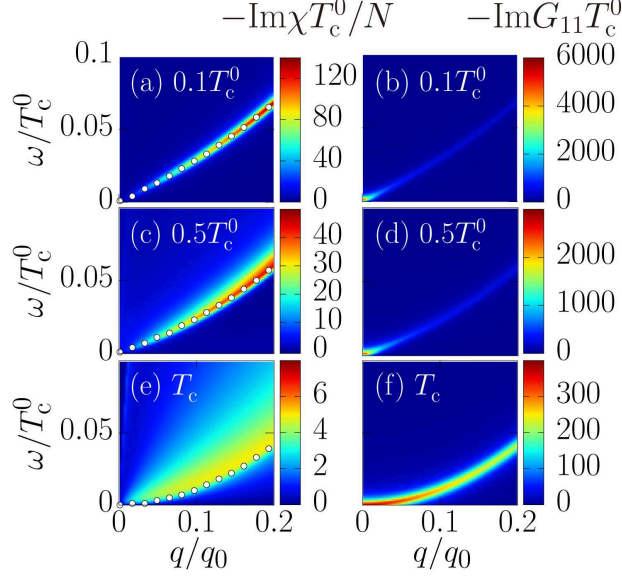


FIG. 12. Momentum and frequency dependence of the total density response function  $\chi$ , and the single-particle Green's function  $G_{11}$ . White points in panels (a), (c), and (e) represent the maximum peak position of  $-\text{Im}G_{11}$ . We used the self-energies in (110) and (111), with the effective interaction (101) including the vertex correction. For the density vertex, we employed  $\Upsilon^s$  and  $\Upsilon^{st}$ . We used the 1PI part in (103) including the vertex correction.

emerges which is not reproduced by the mean-field type Bogoliubov approximation [34]. As temperature increases, the width of the single-particle spectral function becomes broad, and the phonon structure disappears at  $T_c$ . The density response function at higher temperature also becomes quite broad. From these results, we can reasonably expect that it is an essential feature in BECs that the peak position of the density response function overlaps with that of the single-particle Green's function in the very low temperature regime, which is irrespective of the approximation that we take. The linear dispersion at  $T = 0$  is analytically discussed to be originated from the identity  $\partial_\omega \Sigma_{11}(0) = 1$  [36] for the theory satisfying  $\Sigma_{12}(0) = 0$ . In many-body approximations at nonzero temperatures, the numerical analytic continuation makes it difficult to analyze the origin of the structure of the excitation spectrum. Although the linear dispersion can be originated from  $\Sigma_{12}(0)$  in the approximation  $\Sigma_{12}(0) \neq 0$  as discussed in Ref. [1], this problem is important all the more in the many-body approximation at nonzero temperatures satisfying the identity  $\Sigma_{12}(0) = 0$  [34].

The sound speed can be estimated by inversely solving the compressibility zero-frequency

sum-rule  $c = \sqrt{-n/[m\chi(0)]}$ . Since this sum-rule is exhausted by the 1PI part because of  $\chi^{\text{1PR}}(0) = 0$ , the sound speed is exactly given by

$$c = \sqrt{-\frac{n}{m} \frac{1}{\chi^{\text{1PI}}(0)}}. \quad (120)$$

If we employ  $\Upsilon^s$  and  $\Upsilon^{s\dagger}$ , we can reproduce the exact identity  $\chi^{\text{1PR}}(0) = 0$ , because of  $\Upsilon^s(0) = 0$ . The 1PI part (103) in the static and low-momentum limits is given by

$$\chi^{\text{1PI}}(0) = -\frac{1}{U} \frac{1 - U\Pi'(0)}{3 - 2U\Pi'(0)}, \quad (121)$$

and the sound speed at  $T \leq T_c$  can be estimated as

$$c = c_0 \sqrt{\frac{3 - 2U\Pi'(0)}{1 - U\Pi'(0)}}, \quad (122)$$

where  $c_0 \equiv \sqrt{Un/m}$ . This sound speed (122) is found to be a positive real number if we are considering the repulsive interaction  $U > 0$ , because  $\Pi'(0)$  given in (116) is a real negative number according to the relation  $\partial n_{\mathbf{p}}/\partial E_{\mathbf{p}} = -\beta n_{\mathbf{p}}(1 + n_{\mathbf{p}}) < 0$ . At  $T \geq T_c$ , the sound speed is given by

$$c = c_0 \sqrt{\frac{1 - 2U\Pi_{22}(0)}{-U\Pi_{22}(0)}}, \quad (123)$$

where the 1PI part is given in (107). This sound speed (123) is also safely a positive real number for  $U > 0$ , because of the relation

$$\lim_{\mathbf{q} \rightarrow 0} \Pi_{22}(0, \mathbf{q}) = \sum_{\mathbf{p}} \frac{\partial n'_{\mathbf{p}}}{\partial \varepsilon_{\mathbf{p}}} = -\beta \sum_{\mathbf{p}} n'_{\mathbf{p}}(1 + n'_{\mathbf{p}}) < 0. \quad (124)$$

One may employ the simpler regular part (117) for the 1PI part (103). In this bubble diagram case not including the vertex correction, however, we obtain an unphysical temperature-independent sound speed  $c = c_0 = \sqrt{Un/m}$  for all temperatures below  $T_c$ . Since  $\chi_{\text{R}}^s(0)$  exhibits the infrared divergence at  $T \leq T_c$ , the 1PI part (103) in the static and low-momentum limits is temperature-independent, given by  $\chi_{\text{s}}^{\text{1PI}}(0) = -1/U$ .

We discuss the temperature dependence of the sound speed  $c$  using the RPA (122) and (123) (See Fig. 13). In this formalism, the sound speed is temperature dependent, and the sound speeds in (122) and (123) merge at  $T = T_c$ , because of the infrared divergence of the correlation functions  $\Pi'(0)$  and  $\Pi_{22}(0)$  at this temperature. The sound speed is

given by  $c = \sqrt{2}c_0$  at  $T = T_c$  within the RPA including the vertex correction, where the factor 2 comes from the many-body effect in this approximation. In the Bogoliubov-Popov mean-field calculation, the sound speed is given by  $c = \sqrt{Un_0/m}$ , and it drops to zero at the critical temperature. At absolute zero temperature case, the sound speed (122) is approximately given by  $c = \sqrt{3}c_0$  for  $p_c a \ll 1$ . The sound speed is overestimated in the RPA with the vertex correction, although it reproduces the same order of the sound speed in the Bogoliubov approximation at  $T = 0$ . For the consistency, further improvements may be necessary for the calculation of the sound speed derived from the RPA with the zero-frequency compressibility sum-rule.

The sound velocity of the liquid  $^4\text{He}$  has been experimentally studied above the critical temperature [112–115] and below the critical temperature [53, 59, 112–123]. The measurement of the attenuation is also reported [59, 116, 121, 122, 124, 125]. Above the critical temperature, the temperature dependence of the sound velocity is convex [112, 113, 115]. On the other hand, below the critical temperature, the sound velocity is slightly increased for increasing temperature and decreases rapidly near the  $\lambda$ -point [117, 118, 120–122, 124]. The maximum value of the sound velocity is measured around 0.7K [118, 120]. At the critical temperature, the sound velocity shows a cusp anomaly [53, 112, 113, 115, 118, 120–123].

There has been a debate whether the sound speeds below and above the critical temperature converge to the same value or show the discontinuity at the critical temperature in superfluid  $^4\text{He}$ . The measurement of the sound velocity very close to the  $\lambda$ -point has the fundamental difficulty [113, 117, 124]. No detectable discontinuity of the sound velocity was discussed at the  $\lambda$ -transition [112, 113, 124]. The specific heat shows the jump, which suggests the second order phase transition according to the Ehrenfest relations [124], and the isothermal compressibility  $\kappa_T$  shows not the divergence but a discontinuity at the transition point [126]. On the other hand, the logarithmic singularity of  $\kappa_T$  is also discussed at the  $\lambda$ -transition [119, 127]. The sound velocity near the  $\lambda$ -point is also theoretically investigated [96, 97], and ultrasonic attenuation is also studied based on the Pippard–Buckingham–Fairbanks relations [96]. Within the present formalism, the sound speeds converge to the same value from above and below the critical temperature, where it should be noted that thoughtful treatments are needed in fluctuation regions [162].

In the formalism used in this paper, we take the Hartree–Fock–Bogoliubov–Popov approximation  $g(p)$  for constructing the building blocks and self-energies. One of the directions for

the future study is to develop the self-consistent approximation, such as the self-consistent  $T$ -matrix approximation [? ]. In contrast to the Fermi gas, the BEC provides the infrared divergence in the single-particle Green's function with a relation  $G_{11}(0) = -G_{12}(0)$ , which also provides a strong constraint for the infrared divergent polarization functions, given by  $\Pi_{11,22,14}(0) = -\Pi_{12}(0)$  [37]. Since the exact infrared property is important for studying the low-energy properties of the BEC [38], this constraint will be important in development of the self-consistent approximation for the BEC.

The matrix formalism for BECs presented in this paper will have potential to extend theories for the spinor BEC [163], the dipolar BEC [164], the collisionless sound [165], the deep inelastic scattering [166], the Bose polaron problem [167], and the renormalization-group method [48, 145, 157]. Furthermore, ultracold atomic gases may serve as a platform for directly addressing the strong connection between the single-particle and density excitations in BECs by employing useful tools, such as the Feshbach resonance, the uniform box trap, and the Bragg spectroscopy. Theoretical concepts of BECs that should be interesting to confirm experimentally are the Josephson sum-rule, as well as the equivalence of the dispersion relations between the single-particle and collective excitations. It is also interesting to experimentally study the phonon-maxon-roton excitation in dipolar BECs not only in the collective excitation [136], but also in the single-particle excitation below and above the critical temperature by controlling the relative strength of the dipolar to the contact interactions [136], which will provide deeper understanding of the maxon-roton excitations as well as the connection between the single-particle and density excitations in BECs, with extending the context of superfluid  $^4\text{He}$ .

## VIII. CONCLUSIONS

We investigated the single-particle excitation and the collective density excitation in Bose-Einstein condensates (BECs) by using the single-particle Green's function and the density response function. First, we revisited the earlier study presented by Gavoret and Nozières [9], with including the subsequent results given by Nepomnyashchii and Nepomnyashchii [35, 36]. We extended the Nambu representation of the single-particle Green's function for BECs to correlation functions and vertex functions by making the use of the matrix formalism, which reproduces the exact properties efficiently. By following the discus-

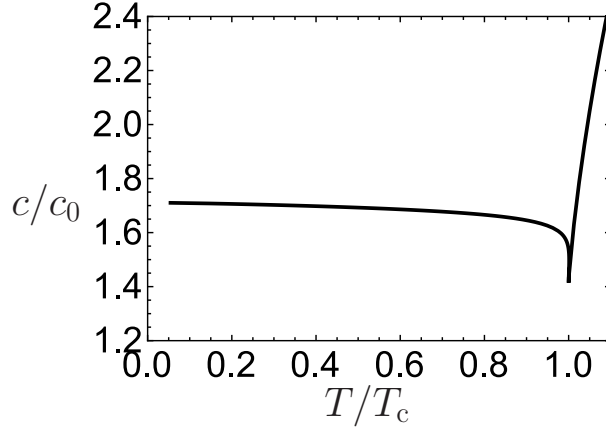


FIG. 13. Sound speed evaluated from the zero-frequency compressibility sum-rule  $c = \sqrt{-n/[m\chi^{\text{PI}}(0)]}$ , scaled by  $c_0 = \sqrt{Un/m}$ . We used the relations (122) and (123) below and above the critical temperature, respectively.

sion given by Gavoret and Nozières [9] with the matrix formalism, we revisited the low-energy properties of the correlation functions and the vertex functions, and the correspondence of the spectrum between the single-particle excitation and the collective excitation in the low-energy and low-momentum regime. We also present an overview of the earlier experimental and theoretical studies on the collective excitations in superfluid  $^4\text{He}$  as well as in ultra-cold atomic gases. We also gave comments on theories casting doubt upon the conventional wisdom of the BEC: the equivalence of the dispersion relations between the single-particle excitation and the collective excitation in the low-energy and low-momentum regime. The consistency of the Bogoliubov operator equality and the Josephson sum-rule is an important criterion for the theory contradict to the conventional wisdom.

By applying the matrix formalism, we developed a random phase approximation (RPA) for BECs to describe a single-particle Green's function and the density response function at nonzero temperatures. Depending on the presence or absence of the vertex correction, approximations provide the quantitatively different temperature dependence of the density response function and the single-particle spectral function. However, the peak positions in both functions are consistent in the very low-temperature regime, which supports the correspondence of the spectrum between the single-particle excitation and the collective excitation. Many-body effect can be seen in the satellite structure of the single-particle spectral function, which comes from the interaction between the condensate and the quasiparticles



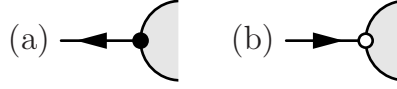


FIG. 14. Function of vertex points ( $\bullet$ ) and ( $\circ$ ). (a) A filled point ( $\bullet$ ) connects to an outgoing external particle line. (b) An open point ( $\circ$ ) connects to an incoming external particle line. A filled point ( $\bullet$ ) can also connect to an open point ( $\circ$ ) and vice versa.

in the medium with the density fluctuation. By using the the compressibility zero-frequency sum-rule, the temperature dependence of the sound speed was evaluated, where the result within the RPA including the vertex correction shows no discontinuity at the critical temperature, although careful treatments are necessary in the fluctuation region.

## ACKNOWLEDGMENTS

Useful conversations with Y. Kato, Y. Ohashi, M. Ueda, and T. Nikuni are acknowledged in the very initial stage of this study. The author thanks A. J. Leggett for providing information about studies by T. Kebukawa and by R. A. Ferrell. He also thanks T. Kita and P. Navez for discussions about theories of BECs. The author was supported by JSPS KAKENHI Grant No. 249416, JP16K17774, JP18K03499.

## Appendix A: Diagrammatic representations and matrix forms of correlation and vertex functions

Correlation and vertex functions are presented in the matrix form in this paper. It is very convenient to explicitly provide these representations in terms of diagrams. We apply the following rules to satisfy the conservation law. The point with the filled circle ( $\bullet$ ) connects to an outgoing external particle line (Fig. 14(a)). The point with the open circle ( $\circ$ ) connects to an incoming external particle line (Fig. 14(b)). The point ( $\bullet$ ) can also connect to the point ( $\circ$ ) and vice versa.

The  $(2 \times 1)$ -matrix vertex functions include the condensate Green's function  $G_{1/2}$ , and the two point vertex  $\Upsilon$  that connects to an external particle line and an external potential line

$$(a) \quad \bullet \text{---} \blacktriangleleft \text{---} \bullet = \begin{pmatrix} \bullet \text{---} \blacktriangleleft \text{---} \\ \circ \text{---} \blacktriangleleft \text{---} \end{pmatrix} \quad (b) \quad \circ \text{---} \Upsilon \text{---} \bullet = \begin{pmatrix} \bullet \text{---} \Upsilon_1 \text{---} \bullet \\ \circ \text{---} \Upsilon_2 \text{---} \bullet \end{pmatrix}$$

FIG. 15.  $(2 \times 1)$ -matrix vertex functions. (a) Condensate Green's function  $G_{1/2}$ . (b) Two point vertex  $\Upsilon$  that connects to an external particle line and an external potential line. A small grey point connects to an external potential line.

$$(a) \quad \bullet \text{---} \blacktriangleleft \text{---} \bullet = \begin{pmatrix} \bullet \text{---} \blacktriangleleft \text{---} \bullet \\ \bullet \text{---} \blacktriangleleft \text{---} \bullet \end{pmatrix} \quad (b) \quad \bullet \text{---} \Upsilon^\dagger \text{---} \bullet = \begin{pmatrix} \bullet \text{---} \Upsilon_1^\dagger \text{---} \bullet \\ \bullet \text{---} \Upsilon_2^\dagger \text{---} \bullet \end{pmatrix}$$

FIG. 16.  $(1 \times 2)$ -matrix vertex functions. (a) Condensate Green's function  $G_{1/2}^\dagger$ . (b) Two point vertex  $\Upsilon^\dagger$  that connects to an external particle line and an external potential line.

(Fig. 15). The  $(1 \times 2)$ -matrix vertex functions  $G_{1/2}^\dagger$  and  $\Upsilon^\dagger$  are their counterparts (Fig. 16).

The  $(2 \times 2)$ -matrix correlation and vertex functions include the single-particle Green's functions  $G_0$  and  $G$ , as well as the self-energy  $\Sigma$  (Fig. 17). These functions are also given in the  $(4 \times 1)$ - or  $(1 \times 4)$ -matrices. The  $(4 \times 1)$ -matrix correlation and vertex functions include the Green's functions  $\mathbf{G}_0$  and  $\mathbf{G}$ , the self-energy  $\mathbf{\Sigma}$ , as well as the three-point vertex  $\gamma$  that connects to two external particle lines and an external interaction line (Fig. 18). The  $(1 \times 4)$ -matrix functions, such as  $\mathbf{G}_0^\dagger$ ,  $\mathbf{G}^\dagger$ ,  $\mathbf{\Sigma}^\dagger$  as well as  $\gamma^\dagger$ , are their counterparts (Fig. 19).

The  $(4 \times 2)$ -matrix vertex functions include the condensate Green's functions  $\mathcal{G}_{1/2}(=\sigma_0 \otimes G_{1/2})$  and  $\hat{T}\mathcal{G}_{1/2}(=G_{1/2} \otimes \sigma_0)$ , as well as the three point vertex  $P$  that connects three external particle lines (Fig. 20). The  $(2 \times 4)$ -matrix vertex functions are their counterparts such as  $\mathcal{G}_{1/2}^\dagger(=\sigma_0 \otimes G_{1/2}^\dagger)$ ,  $\mathcal{G}_{1/2}^\dagger \hat{T}(=G_{1/2}^\dagger \otimes \sigma_0)$  as well as  $P^\dagger$  (Fig. 21). The  $(4 \times 4)$ -matrix correlation and vertex functions include the four-point vertex  $\Gamma$ , as well as the two-particle Green's functions, given by  $K$ ,  $K_0$  and  $K_0 \hat{T}$  (Figs. 22 and 23).

The matrix  $\hat{T}$  may provide exchange contributions of the two-particle Green's function. In the diagram of  $\hat{T}K_0$  ( $K_0 \hat{T}$ ), upper and lower left (right) ends of the two-particle Green's function  $K_0$  are exchanged (Fig. 23). The condensate Green's function  $\mathcal{G}_{1/2}^\dagger$  ( $\mathcal{G}_{1/2}$ ) connects to lower left (right) corner of the four-point vertex  $\Gamma$ . The condensate Green's function  $\mathcal{G}_{1/2}^\dagger \hat{T}$  ( $\hat{T} \mathcal{G}_{1/2}$ ) connects to upper left (right) corner of  $\Gamma$ . The matrix  $\hat{T}$  works as  $\hat{T}(\sigma_0 \otimes G_{1/2}) =$

$$\begin{aligned}
\text{(a)} \quad \overline{\overline{G_0(p)}} &= \begin{pmatrix} \overleftarrow{G^{(0)}(p)} & 0 \\ 0 & \overrightarrow{G^{(0)}(-p)} \end{pmatrix} \\
\text{(b)} \quad \overline{\overline{G(p)}} &= \begin{pmatrix} \overleftarrow{G_{11}} & \overleftrightarrow{G_{12}} \\ \overleftrightarrow{G_{21}} & \overrightarrow{G_{22}} \end{pmatrix} \\
\text{(c)} \quad \text{circle with } \Sigma(p) &= \begin{pmatrix} \text{circle with } \Sigma_{11} & \text{circle with } \Sigma_{12} \\ \text{circle with } \Sigma_{21} & \text{circle with } \Sigma_{22} \end{pmatrix}
\end{aligned}$$

FIG. 17.  $(2 \times 2)$ -matrix correlation and vertex functions. (a) Free-part of the single-particle Green's function  $G_0$ . (b) Single-particle Green's function  $G$ . (c) Self-energy  $\Sigma$ .

$$\begin{aligned}
\text{(a)} \quad \overline{\overline{\mathbf{G}_0(p)}} &= \begin{pmatrix} 0 & \uparrow G^{(0)}(p) \\ \downarrow G^{(0)}(-p) & 0 \end{pmatrix} \\
\text{(b)} \quad \overline{\overline{\mathbf{G}(p)}} &= \begin{pmatrix} \updownarrow G_{12} \\ \uparrow G_{11} \\ \downarrow G_{22} \\ \updownarrow G_{21} \end{pmatrix} \\
\text{(c)} \quad \text{circle with } \Sigma(p) &= \begin{pmatrix} \text{circle with } \Sigma_{12} \\ \text{circle with } \Sigma_{11} \\ \text{circle with } \Sigma_{22} \\ \text{circle with } \Sigma_{21} \end{pmatrix} \\
\text{(d)} \quad \text{triangle with } \gamma &= \begin{pmatrix} \text{triangle with } \gamma_1 \\ \text{triangle with } \gamma_2 \\ \text{triangle with } \gamma_3 \\ \text{triangle with } \gamma_4 \end{pmatrix}
\end{aligned}$$

FIG. 18.  $(4 \times 1)$ -matrix correlation and vertex functions. (a) Free-part of the single-particle Green's function  $\mathbf{G}_0$ . (b) Single-particle Green's function  $\mathbf{G}$ . (c) Self-energy  $\Sigma$ . (d) Three-point vertex  $\gamma$  that connects to two external particle lines and an external interaction line.

$$G_{1/2} \otimes \sigma_0 \text{ as well as } (\sigma_0 \otimes G_{1/2}^\dagger) \hat{T} = G_{1/2}^\dagger \otimes \sigma_0.$$

The density and current correlation functions  $\chi_{\mu\nu}$  are obtained by multiplying the two-particle Green's function  $K$  by the density and current vertex vectors  $\langle \lambda_\mu |$  and  $|\lambda_\nu \rangle$  from its left- and right-hand sides, respectively. In the diagrammatic representation,  $\langle \lambda_\mu |$  (or  $|\lambda_\nu \rangle$ ) closes leftmost (or rightmost) of  $K$  with multiplying it by the vertex function  $\lambda_\mu$  (or  $\lambda_\nu$ ) (Fig. 3). In particular, since  $|\lambda_0 \rangle = |f_0 \rangle$ , the density response function are obtained by multiplying  $K$  by  $\langle f_0 |$  and  $|f_0 \rangle$  from its left- and right-hand sides, respectively, which generate vertex points connecting to the external potential line. These factors  $\langle f_0 |$  and  $|f_0 \rangle$  also provides the relations  $\mathcal{G}_{1/2}^\dagger |f_0 \rangle = \mathcal{G}_{1/2}^\dagger \hat{T} |f_0 \rangle = G_{1/2}$  and  $\langle f_0 | \mathcal{G}_{1/2} = \langle f_0 | \hat{T} \mathcal{G}_{1/2} = G_{1/2}^\dagger$ .

$$\begin{aligned}
\text{(a)} \quad \left\| \right\| &= \begin{pmatrix} 0, & \downarrow, & \uparrow, & 0 \end{pmatrix} \\
&\quad \mathbf{G}_0^\dagger(p) \quad G^{(0)}(p) \quad G^{(0)}(-p) \\
\text{(b)} \quad \left\| \right\| &= \begin{pmatrix} \uparrow\downarrow, & \downarrow, & \uparrow, & \uparrow\downarrow \end{pmatrix} \\
&\quad \mathbf{G}^\dagger(p) \quad G_{21} \quad G_{11} \quad G_{22} \quad G_{12} \\
\text{(c)} \quad \bigcirc &= \left( \bigcirc, \bigcirc, \bigcirc, \bigcirc \right) \\
&\quad \Sigma^\dagger(p) \quad \Sigma_{21} \quad \Sigma_{11} \quad \Sigma_{22} \quad \Sigma_{12} \\
\text{(d)} \quad \triangle &= \left( \triangle, \triangle, \triangle, \triangle \right) \\
&\quad \gamma^\dagger \quad \gamma_1^\dagger \quad \gamma_2^\dagger \quad \gamma_3^\dagger \quad \gamma_4^\dagger
\end{aligned}$$

FIG. 19.  $(1 \times 4)$ -matrix correlation and vertex functions. (a) Free-part of the single-particle Green's function  $\mathbf{G}_0^\dagger$ . (b) Single-particle Green's function  $\mathbf{G}^\dagger$ . (c) Self-energy  $\Sigma^\dagger$ . (d) Three-point vertex  $\gamma^\dagger$  that connects to two external particle lines and an external interaction line.

$$\begin{aligned}
\text{(a)} \quad \bullet \rightleftharpoons \bullet &= \begin{pmatrix} \bullet \dashrightarrow & 0 \\ \circ \dashrightarrow & 0 \\ 0 & \bullet \dashrightarrow \\ 0 & \circ \dashrightarrow \end{pmatrix} \\
\text{(b)} \quad \bullet \rightleftharpoons \bullet &= \begin{pmatrix} \bullet \dashrightarrow & 0 \\ 0 & \bullet \dashrightarrow \\ \circ \dashrightarrow & 0 \\ 0 & \circ \dashrightarrow \end{pmatrix} \\
\text{(c)} \quad \triangle &= \begin{pmatrix} \triangle P_{11} & \triangle P_{12} \\ \triangle P_{21} & \triangle P_{22} \\ \triangle P_{31} & \triangle P_{32} \\ \triangle P_{41} & \triangle P_{42} \end{pmatrix}
\end{aligned}$$

FIG. 20. The  $(4 \times 2)$ -matrix vertex functions. (a) Condensate Green's function  $\mathcal{G}_{1/2} = \sigma_0 \otimes G_{1/2}$ . (b)  $\hat{T}\mathcal{G}_{1/2} = G_{1/2} \otimes \sigma_0$ . (c) Three point vertex  $P$  that connects to three external particle lines. The matrix  $Q$  as well as the 2PI part  $J$  of the three point vertex  $P$  are also given in the same matrix form.

## Appendix B: Thermodynamic relations

We summarize thermodynamic relations with the use of the Nepomnyashchii–Nepomnyashchii identity (43). We also show relations with respect to the isothermal sound speed  $c_T$ .

Since the thermodynamic potential  $\Omega' = -T \ln \Xi$  is related to the grand potential  $\Omega$  through  $\Omega' = \Omega + \mu_0 n_0$ , we have a relation

$$d\Omega'(T, \mu, n_0) = -SdT - n'd\mu + \mu_0 dn_0, \quad (\text{B1})$$

where the volume of the system is assumed to be fixed. Here, the entropy  $S$ , the non-

$$\begin{aligned}
\text{(a)} \quad \mathcal{G}_{1/2}^\dagger &= \begin{pmatrix} \text{---}\leftarrow\text{---}\circ & \text{---}\rightarrow\text{---}\bullet & 0 & 0 \\ 0 & 0 & \text{---}\leftarrow\text{---}\circ & \text{---}\rightarrow\text{---}\bullet \end{pmatrix} \\
\text{(b)} \quad \mathcal{G}_{1/2}^\dagger \hat{T} &= \begin{pmatrix} \text{---}\leftarrow\text{---}\circ & 0 & \text{---}\rightarrow\text{---}\bullet & 0 \\ 0 & \text{---}\leftarrow\text{---}\circ & 0 & \text{---}\rightarrow\text{---}\bullet \end{pmatrix} \\
\text{(c)} \quad P^\dagger &= \begin{pmatrix} \text{---}\leftarrow\text{---}\circ & \text{---}\rightarrow\text{---}\bullet & \text{---}\leftarrow\text{---}\circ & \text{---}\rightarrow\text{---}\bullet \\ \text{---}\leftarrow\text{---}\circ & \text{---}\rightarrow\text{---}\bullet & \text{---}\leftarrow\text{---}\circ & \text{---}\rightarrow\text{---}\bullet \\ \text{---}\leftarrow\text{---}\circ & \text{---}\rightarrow\text{---}\bullet & \text{---}\leftarrow\text{---}\circ & \text{---}\rightarrow\text{---}\bullet \\ \text{---}\leftarrow\text{---}\circ & \text{---}\rightarrow\text{---}\bullet & \text{---}\leftarrow\text{---}\circ & \text{---}\rightarrow\text{---}\bullet \end{pmatrix}
\end{aligned}$$

FIG. 21. The  $(2 \times 4)$ -matrix vertex functions. (a) Condensate Green's function  $\mathcal{G}_{1/2}^\dagger = \sigma_0 \otimes G_{1/2}^\dagger$ . (b)  $\mathcal{G}_{1/2}^\dagger \hat{T} = G_{1/2}^\dagger \otimes \sigma_0$ . (c) Three point vertex  $P^\dagger$  that connects to three external particle lines. The matrix  $Q^\dagger$  as well as the 2PI part  $J^\dagger$  of the three point vertex  $P^\dagger$  are also given in the same matrix form.

$$\begin{aligned}
\text{(a)} \quad \Gamma &= \begin{pmatrix} \Gamma_{11} & \Gamma_{12} & \Gamma_{13} & \Gamma_{14} \\ \Gamma_{21} & \Gamma_{22} & \Gamma_{23} & \Gamma_{24} \\ \Gamma_{31} & \Gamma_{32} & \Gamma_{33} & \Gamma_{34} \\ \Gamma_{41} & \Gamma_{42} & \Gamma_{43} & \Gamma_{44} \end{pmatrix} \\
\text{(b)} \quad K_0 &= \begin{pmatrix} \text{---}\leftarrow\text{---} & \text{---}\leftarrow\text{---} & \text{---}\rightarrow\text{---} & \text{---}\rightarrow\text{---} \\ \text{---}\leftarrow\text{---} & \text{---}\leftarrow\text{---} & \text{---}\rightarrow\text{---} & \text{---}\rightarrow\text{---} \\ \text{---}\rightarrow\text{---} & \text{---}\rightarrow\text{---} & \text{---}\leftarrow\text{---} & \text{---}\leftarrow\text{---} \\ \text{---}\rightarrow\text{---} & \text{---}\rightarrow\text{---} & \text{---}\leftarrow\text{---} & \text{---}\leftarrow\text{---} \end{pmatrix}
\end{aligned}$$

FIG. 22.  $(4 \times 4)$ -matrix correlation and vertex functions. (a) Four-point vertex  $\Gamma$  that connects to four external particle lines. The 2PI part  $I$  of the four point vertex  $\Gamma$  is also given in the same matrix form. (b) Bare part of the two-particle Green's function  $K_0$ .

condensate density  $n'$  and the chemical potential of the condensate  $\mu_0$ , which satisfies  $\mu = \mu_0$ , are respectively given by

$$S = -\frac{\partial \Omega'}{\partial T}, \quad n' = -\frac{\partial \Omega'}{\partial \mu}, \quad \mu_0 = \frac{\partial \Omega'}{\partial n_0}. \quad (\text{B2})$$

A thermodynamic relation provides

$$\begin{aligned}
& d\mu_0(T, \mu, n_0) \\
&= \left. \frac{\partial \mu_0}{\partial T} \right|_{\mu, n_0} dT + \left. \frac{\partial \mu_0}{\partial \mu} \right|_{T, n_0} d\mu + \left. \frac{\partial \mu_0}{\partial n_0} \right|_{T, \mu} dn_0.
\end{aligned} \quad (\text{B3})$$

$$K_0 \hat{T} = \begin{pmatrix} \text{crossed double line with arrows} & \text{crossed double line with arrows} & \text{crossed double line with arrows} & \text{crossed double line with arrows} \\ \text{crossed double line with arrows} & \text{crossed double line with arrows} & \text{crossed double line with arrows} & \text{crossed double line with arrows} \\ \text{crossed double line with arrows} & \text{crossed double line with arrows} & \text{crossed double line with arrows} & \text{crossed double line with arrows} \\ \text{crossed double line with arrows} & \text{crossed double line with arrows} & \text{crossed double line with arrows} & \text{crossed double line with arrows} \end{pmatrix}$$

FIG. 23. Effect of the matrix  $\hat{T}$  on bare part of the two-particle Green's function  $K_0$ .

By using the relations  $d\mu_0 = d\mu$  and  $\partial\Omega'/(\partial T \partial n_0) = \partial\mu_0/\partial T|_{\mu, n_0} = -\partial S/\partial n_0|_{\mu, n_0}$ , as well as the Nepomnyashchii–Nepomnyashchii identity (43), we obtain identities

$$\frac{\partial^2 \Omega'}{\partial \mu \partial n_0} = \frac{\partial \mu_0}{\partial \mu} \Big|_{T, n_0} = - \frac{\partial n'}{\partial n_0} \Big|_{T, \mu} = 1 + \frac{\partial S}{\partial n_0} \Big|_{T, \mu} \frac{dT}{d\mu}. \quad (\text{B4})$$

Given (38) as well as (B4), we have

$$\Upsilon_0(0) = - \sqrt{n_0} \frac{\partial S}{\partial n_0} \Big|_{T, \mu} \frac{dT}{d\mu} |+\rangle, \quad (\text{B5})$$

In the isothermal condition, we end with  $\Upsilon_0(0) = 0$  as shown in (45).

We also have other thermodynamic relation

$$dn(T, \mu, n_0) = \frac{\partial n}{\partial T} \Big|_{\mu, n_0} dT + \frac{\partial n}{\partial \mu} \Big|_{T, n_0} d\mu + \frac{\partial n}{\partial n_0} \Big|_{T, \mu} dn_0. \quad (\text{B6})$$

Since  $n_0$  is fixed in the first and second terms in (B6), we have relations  $\partial n/\partial T|_{\mu, n_0} = \partial n'/\partial T|_{\mu, n_0} = \partial S/\partial \mu|_{T, n_0}$  and  $(\partial n/\partial \mu)_{n_0} = (\partial n'/\partial \mu)_{n_0}$ . Since  $n = n_0 + n'$ , we also have

$$\frac{\partial n}{\partial n_0} \Big|_{T, \mu} = 1 + \frac{\partial n'}{\partial n_0} \Big|_{T, \mu} = - \frac{\partial S}{\partial n_0} \Big|_{T, \mu} \frac{dT}{d\mu}, \quad (\text{B7})$$

where we applied (B4) to the last equality. The thermodynamic relation is reduced into

$$\frac{dn}{d\mu} = \frac{\partial n'}{\partial \mu} \Big|_{T, n_0} + \left( \frac{\partial S}{\partial \mu} \Big|_{T, n_0} - \frac{\partial S}{\partial n_0} \Big|_{T, \mu} \frac{dn_0}{d\mu} \right) \frac{dT}{d\mu} \quad (\text{B8})$$

As a result, we have a thermodynamic relation with respect to the isothermal sound speed  $c_T$ , giving the form

$$\frac{n}{mc_T^2} = \frac{dn}{d\mu} \Big|_T = \frac{\partial n'}{\partial \mu} \Big|_{T, n_0} = - \frac{\partial^2 \Omega}{\partial \mu^2}, \quad (\text{B9})$$

where the second equality is obtained from (B8) with the isothermal condition.

## Appendix C: Derivation of the low-energy behavior of the single-particle Green's function including the non-analytic term $\Delta\Sigma$

The Dyson equation (9) provides the single-particle Green's function, given in the form

$$G(p) = \frac{1}{D(p)}[\omega\sigma_3 + \varepsilon_{\mathbf{p}} - \mu + \sigma_3\Sigma(-p)\sigma_3], \quad (\text{C1})$$

where

$$D(p) \equiv \frac{1}{4}[D_0^2(p) - D_+(p)D_-(p)], \quad (\text{C2})$$

with  $D_0(p) \equiv \text{Tr}[\omega - \sigma_3\Sigma(p)]$  and  $D_{\pm}(p) \equiv \langle \pm | [\varepsilon_{\mathbf{p}} - \mu + \Sigma(p)] | \pm \rangle$ . In the low energy regime, by using (58), (60) as well as (61), we have  $D_0(p) = O(p^2)$ , as well as

$$D_+(p) \simeq 4\Delta\Sigma(p) \simeq 4\Sigma_{12}(p), \quad (\text{C3})$$

$$\begin{aligned} D_-(p) &\simeq \frac{1}{2} \langle - | \partial_{\omega}^2 \Sigma'(0) | - \rangle \omega^2 + \left[ \frac{1}{m} + \frac{1}{2} \langle - | \partial_{\mathbf{p}}^2 \Sigma'(0) | - \rangle \right] \mathbf{p}^2 \\ &= - \frac{n}{n_0 m c_{\text{T}}^2} (\omega^2 - c_{\text{T}}^2 \mathbf{p}^2). \end{aligned} \quad (\text{C4})$$

In the last equality of (C3), we used the fact that the leading term of the off-diagonal self-energy  $\Sigma_{12}$  is the nonanalytic part  $\Delta\Sigma(p)$  in the small  $p$  regime. As a consequence, the low-energy behavior (62) is conveniently obtained by using relations

$$\begin{pmatrix} G_{11} \pm G_{12} \\ G_{21} \pm G_{22} \end{pmatrix} = G(p) | \pm \rangle = \simeq - \frac{2}{D_{\pm}(p)} | \pm \rangle, \quad (\text{C5})$$

which provides  $G_{11,22} = -1/D_- - 1/D_+$  as well as  $G_{12,21} = +1/D_- - 1/D_+$ . As a result, we end with Eq. (62).

## Appendix D: derivations of (57) and (66)-(69)

### 1. derivations of (57)

An element of the density and current vertices are given by

$$\gamma_{\mu}(q) = \frac{1}{2} [\Upsilon_{\mu}^{\dagger}(q) | 0 \rangle + \Upsilon_{\mu}^{\dagger}(-q) | 1 \rangle], \quad (\text{D1})$$

where we used the symmetry relations (56). Using (34), we find that

$$\begin{aligned}\gamma_\mu(q) = & -\frac{1}{2}T \sum_p \langle \lambda_\mu(p; q) | Q(p; q) | 0 \rangle \\ & -\frac{1}{2}T \sum_p \langle \lambda_\mu(p; -q) | Q(p; -q) | 1 \rangle.\end{aligned}\quad (\text{D2})$$

Given (20) as well as (46), this vertex is constructed from three parts:

$$\gamma_\mu(q) = \gamma_\mu^{(1)}(q) + \gamma_\mu^{(2)}(q) + \gamma_\mu^{(3)}(q), \quad (\text{D3})$$

where

$$\begin{aligned}\gamma_\mu^{(1)}(q) = & -\frac{1}{4}\sqrt{-1}[\langle \lambda_\mu(0; q) | \mathcal{G}_{1/2} | 0 \rangle \\ & + \langle \lambda_\mu(0; -q) | \mathcal{G}_{1/2} | 1 \rangle],\end{aligned}\quad (\text{D4})$$

$$\begin{aligned}\gamma_\mu^{(2)}(q) = & -\frac{1}{4}\sqrt{-1}[\langle \lambda_\mu(-q; q) | \hat{T} \mathcal{G}_{1/2} | 0 \rangle \\ & + \langle \lambda_\mu(q; -q) | \hat{T} \mathcal{G}_{1/2} | 1 \rangle],\end{aligned}\quad (\text{D5})$$

$$\begin{aligned}\gamma_\mu^{(3)}(q) = & -\frac{1}{4}T \sum_p [\langle \lambda_\mu(p; q) | L(p; q) | 0 \rangle \\ & + \langle \lambda_\mu(p; -q) | L(p; -q) | 1 \rangle].\end{aligned}\quad (\text{D6})$$

The terms  $\gamma_\mu^{(1)}(q)$  and  $\gamma_\mu^{(2)}(q)$  is reduced to

$$\gamma_\mu^{(1)}(q) = \gamma_\mu^{(2)}(q) = \frac{1}{2}\lambda_\mu(0; q)\sqrt{n_0}, \quad (\text{D7})$$

where we used relations  $\lambda_\mu(0; -q) = f_\mu \lambda_\mu(0; q)$ ,  $\lambda_\mu(\mp q; \pm q) = \lambda_\mu(0; \mp q)$  as well as  $\langle f_\mu | \mathcal{G}_{1/2} | 0 \rangle = \langle f_\mu | \hat{T} \mathcal{G}_{1/2} | 1 \rangle = f_\mu \langle f_\mu | \mathcal{G}_{1/2} | 1 \rangle = f_\mu \langle f_\mu | \hat{T} \mathcal{G}_{1/2} | 0 \rangle = \sqrt{-n_0}$ . The sum of these two terms  $\gamma_\mu^{(1)} + \gamma_\mu^{(2)}$  provides the first term of (57).

The term  $\gamma_\mu^{(3)}(q)$  in the first order of  $q$  is given by

$$\gamma_\mu^{(3)}(q) \simeq -\frac{T}{4} \sum_p \lambda_\mu(p; 0) [\langle f_\mu | L(p; q) | 0 \rangle + \langle f_\mu | L(p; -q) | 1 \rangle], \quad (\text{D8})$$

where we have used  $\langle f_\mu | L(p; 0) | 0 \rangle = \langle f_\mu | L(p; 0) | 1 \rangle$  as well as  $\lambda_i(p; \pm q) = \lambda_i(p; 0) \pm \lambda_i(0; q)$  for  $i = 1, 2, 3$ . Using (48), we find

$$\begin{aligned}\gamma_\mu^{(3)}(q) \simeq & -\frac{T}{4} \sum_p \lambda_\mu(p; 0) \\ & \times [\mathcal{D}_1(q) \langle f_\mu | \mathbf{G}(p) + \mathcal{D}_2(q) \langle f_\mu | \hat{B} \mathbf{G}(p)].\end{aligned}\quad (\text{D9})$$



By using (D9) as well as the following two mathematical identities

$$\langle f_\mu | \mathbf{G}(p) = \text{Tr}[\sigma'_\mu G(p)], \quad \langle f_\mu | \hat{B} \mathbf{G}(p) = -\text{Tr}[\sigma'_\mu \sigma_3 G(p)], \quad (\text{D10})$$

we obtain the second term of (57). We can thus obtain (57).

We can also derive the same result by using

$$\gamma_\mu(q) = \frac{1}{2}[\langle 0 | \Upsilon_\mu(q) + \langle 1 | \Upsilon_\mu(-q)]. \quad (\text{D11})$$

In this case, we apply a variant of (48), giving the form

$$\langle 0 | L^\dagger(p, +q) + \langle 1 | L^\dagger(p, -q) \simeq \hat{\mathcal{D}}(q) \mathbf{G}^\dagger(p), \quad (\text{D12})$$

where  $L^\dagger(p; q) = P^\dagger(p; q) K_0(p; q)$ . We also apply the mathematical identities

$$\mathbf{G}^\dagger(p) | f_\mu \rangle = \text{Tr}[\sigma'_\mu G(p)], \quad \mathbf{G}^\dagger(p) \hat{B} | f_\mu \rangle = -\text{Tr}[\sigma'_\mu \sigma_3 G(p)], \quad (\text{D13})$$

as well as  $\langle 0 | \mathcal{G}_{1/2}^\dagger | f_\mu \rangle = \langle 1 | \mathcal{G}_{1/2}^\dagger \hat{T} | f_\mu \rangle = f_\mu \langle 1 | \mathcal{G}_{1/2}^\dagger | f_\mu \rangle = f_\mu \langle 0 | \mathcal{G}_{1/2}^\dagger \hat{T} | f_\mu \rangle = \sqrt{-n_0}$ .

## 2. derivations of (66)-(69)

We derive the low energy behavior of the 1PI part  $\chi_{\mu\nu}^{\text{1PI}}$ . First, we can reduce Eq. (31) into

$$\chi_{\mu\nu}^{\text{1PI}}(q) = -\frac{1}{2}T \sum_p \langle \lambda_\mu(p; q) | K_0(p; q) | \Lambda_\nu(p; q) \rangle, \quad (\text{D14})$$

where we introduced the density and current vertex vector with the vertex corrections, given by

$$|\Lambda_\nu(p; q) \rangle = |\lambda_\nu(p; q) \rangle - T \sum_{p'} \Gamma(p, p'; q) K_0(p'; q) |\lambda_\nu(p'; q) \rangle. \quad (\text{D15})$$

To obtain this form, we used relations  $\hat{T}^2 = 1$  and

$$\hat{T} |\lambda_\nu(-p - q; q) \rangle = |\lambda_\nu(p; q) \rangle, \quad (\text{D16})$$

$$\hat{T} K_0(-p - q; q) \hat{T} = K_0(p; q). \quad (\text{D17})$$

The density and current vertex at  $q = 0$  can be reduced into

$$|\Lambda_\nu(p; 0) \rangle = |\lambda_\nu(p; 0) \rangle - f_\nu \frac{\delta}{\delta x_\nu} \Sigma(p). \quad (\text{D18})$$

$$\frac{\delta}{\delta x_\nu} \Sigma = f_\nu \times \left[ \Gamma \text{ (rectangle)} \text{ --- } \text{G (semi-circle)} \text{ --- } \lambda_\nu \right]^{K_0 | f_\nu \rangle}$$

FIG. 24. Diagrammatic representation of (D19).

The two point vertex  $\Sigma$  is given by the four point vertex  $\Gamma$ , where two of four vertex points are blocked by the single-particle Green's function  $\mathbf{G}$ . By taking the derivative  $\delta/\delta x_\nu$ , we have [9]

$$\frac{\delta}{\delta x_\nu} \Sigma(p) = f_\nu T \sum_{p'} \Gamma(p, p'; 0) K_0(p'; 0) |\lambda_\nu(p'; 0)\rangle, \quad (\text{D19})$$

which is diagrammatically described in Fig. 24. The factor  $f_\nu \lambda(p; 0)$  as well as the bare part of the two-particle Green's function  $K_0$  come from a relation  $\delta G_0(p)/\delta x_\nu = -f_\nu \lambda(p; 0) G_0^2(p)$  [9].

The 1PI part  $\chi_{\mu\nu}^{1\text{PI}}$  is then given in the form

$$\begin{aligned} \chi_{\mu\nu}^{1\text{PI}}(0) = & -\frac{1}{2} T \sum_p \langle \lambda_\mu(p; 0) | K_0(p; 0) | \lambda_\nu(p; 0) \rangle \\ & + \frac{1}{2} T \sum_p \langle \lambda_\mu(p; 0) | K_0(p; 0) f_\nu \frac{\delta}{\delta x_\nu} \Sigma(p) \rangle. \end{aligned} \quad (\text{D20})$$

We may also have two mathematical identities

$$\langle \lambda_\mu(p; 0) | K_0(p; 0) | \lambda_\nu(p; 0) \rangle = \lambda_\mu(p; 0) \lambda_\nu(p; 0) \text{Tr} [\sigma'_\mu G(p) \sigma'_\nu G(p)], \quad (\text{D21})$$

$$\langle f_\mu | K_0(p; 0) \frac{\delta}{\delta x_\nu} \Sigma(p) = \text{Tr} \left[ \sigma'_\mu G(p) \frac{\delta \Sigma(p)}{\delta x_\nu} G(p) \right]. \quad (\text{D22})$$

Given these identities, we may reduce  $\chi_{\mu\nu}^{1\text{PI}}(0)$  into

$$\begin{aligned} \chi_{\mu\nu}^{1\text{PI}}(0) = & -\frac{1}{2} T \sum_p \text{Tr} \left\{ f_\nu \lambda_\mu(p; 0) \sigma'_\mu G(p) \right. \\ & \times \left[ f_\nu \lambda_\nu(p; 0) \sigma'_\nu - \frac{\delta \Sigma(p)}{\delta x_\nu} \right] G(p) \left. \right\}. \end{aligned} \quad (\text{D23})$$

From the Dyson-Beliaev equation  $G = G_0 + G_0 \Sigma G$ , we can derive [9]

$$\frac{\delta G(p)}{\delta x_\nu} = -G(p) \left[ \frac{\delta G_0^{-1}(p)}{\delta x_\nu} - \frac{\delta \Sigma(p)}{\delta x_\nu} \right] G(p). \quad (\text{D24})$$

In particular, we have

$$\frac{\delta G_0^{-1}(p)}{\delta x_\nu} = f_\nu \lambda_\nu(p; 0) \sigma'_\nu. \quad (\text{D25})$$

By applying these two relations (D24) and (D25) to (D23), we end with

$$\chi_{\mu\nu}^{\text{1PI}}(0) = \frac{1}{2} T \sum_p f_\nu \lambda_\mu(p; 0) \frac{\delta}{\delta x_\nu} \text{Tr}[\sigma'_\mu G(p)], \quad (\text{D26})$$

where

$$\sigma'_\mu = \begin{pmatrix} 1 & 0 \\ 0 & f_\mu \end{pmatrix}. \quad (\text{D27})$$

This relation provides (66), (67), (68), and (69).

## Appendix E: Polarization Functions

We summarize the polarization functions for the random-phase approximation studied in this paper [37–39]. At  $T \leq T_c$ , the polarization functions are given by

$$\begin{aligned} \Pi_{11}(q) = & - \sum_{\mathbf{p}} \frac{1}{2} \left[ (E_{\mathbf{p}+\mathbf{q}} - E_{\mathbf{p}}) \left( 1 - \frac{\xi_{\mathbf{p}+\mathbf{q}} \xi_{\mathbf{p}}}{E_{\mathbf{p}+\mathbf{q}} E_{\mathbf{p}}} \right) + i\omega_n \left( \frac{\xi_{\mathbf{p}+\mathbf{q}}}{E_{\mathbf{p}+\mathbf{q}}} - \frac{\xi_{\mathbf{p}}}{E_{\mathbf{p}}} \right) \right] \frac{n_{\mathbf{p}+\mathbf{q}} - n_{\mathbf{p}}}{\omega_n^2 + (E_{\mathbf{p}+\mathbf{q}} - E_{\mathbf{p}})^2} \\ & - \sum_{\mathbf{p}} \frac{1}{2} \left[ (E_{\mathbf{p}+\mathbf{q}} + E_{\mathbf{p}}) \left( 1 + \frac{\xi_{\mathbf{p}+\mathbf{q}} \xi_{\mathbf{p}}}{E_{\mathbf{p}+\mathbf{q}} E_{\mathbf{p}}} \right) + i\omega_n \left( \frac{\xi_{\mathbf{p}+\mathbf{q}}}{E_{\mathbf{p}+\mathbf{q}}} + \frac{\xi_{\mathbf{p}}}{E_{\mathbf{p}}} \right) \right] \frac{1 + n_{\mathbf{p}+\mathbf{q}} + n_{\mathbf{p}}}{\omega_n^2 + (E_{\mathbf{p}+\mathbf{q}} + E_{\mathbf{p}})^2}, \end{aligned} \quad (\text{E1})$$

$$\begin{aligned} \Pi_{12}(q) = & - \sum_{\mathbf{p}} \frac{1}{2} \Delta \left[ \frac{\xi_{\mathbf{p}+\mathbf{q}}}{E_{\mathbf{p}+\mathbf{q}} E_{\mathbf{p}}} (E_{\mathbf{p}+\mathbf{q}} - E_{\mathbf{p}}) + \frac{i\omega_n}{E_{\mathbf{p}}} \right] \frac{n_{\mathbf{p}+\mathbf{q}} - n_{\mathbf{p}}}{\omega_n^2 + (E_{\mathbf{p}+\mathbf{q}} - E_{\mathbf{p}})^2} \\ & + \sum_{\mathbf{p}} \frac{1}{2} \Delta \left[ \frac{\xi_{\mathbf{p}+\mathbf{q}}}{E_{\mathbf{p}+\mathbf{q}} E_{\mathbf{p}}} (E_{\mathbf{p}+\mathbf{q}} + E_{\mathbf{p}}) + \frac{i\omega_n}{E_{\mathbf{p}}} \right] \frac{1 + n_{\mathbf{p}+\mathbf{q}} + n_{\mathbf{p}}}{\omega_n^2 + (E_{\mathbf{p}+\mathbf{q}} + E_{\mathbf{p}})^2}, \end{aligned} \quad (\text{E2})$$

$$\Pi_{14}(q) = \sum_{\mathbf{p}} \frac{1}{2} \frac{\Delta^2}{E_{\mathbf{p}+\mathbf{q}} E_{\mathbf{p}}} \left[ (E_{\mathbf{p}+\mathbf{q}} - E_{\mathbf{p}}) \frac{n_{\mathbf{p}+\mathbf{q}} - n_{\mathbf{p}}}{\omega_n^2 + (E_{\mathbf{p}+\mathbf{q}} - E_{\mathbf{p}})^2} - (E_{\mathbf{p}+\mathbf{q}} + E_{\mathbf{p}}) \frac{1 + n_{\mathbf{p}+\mathbf{q}} + n_{\mathbf{p}}}{\omega_n^2 + (E_{\mathbf{p}+\mathbf{q}} + E_{\mathbf{p}})^2} \right], \quad (\text{E3})$$

$$\begin{aligned} \Pi_{22}(q) = & \sum_{\mathbf{p}} \frac{1}{2} \left[ (E_{\mathbf{p}+\mathbf{q}} - E_{\mathbf{p}}) \left( 1 + \frac{\xi_{\mathbf{p}+\mathbf{q}} \xi_{\mathbf{p}}}{E_{\mathbf{p}+\mathbf{q}} E_{\mathbf{p}}} \right) + i\omega_n \left( \frac{\xi_{\mathbf{p}+\mathbf{q}}}{E_{\mathbf{p}+\mathbf{q}}} + \frac{\xi_{\mathbf{p}}}{E_{\mathbf{p}}} \right) \right] \frac{n_{\mathbf{p}+\mathbf{q}} - n_{\mathbf{p}}}{\omega_n^2 + (E_{\mathbf{p}+\mathbf{q}} - E_{\mathbf{p}})^2} \\ & + \sum_{\mathbf{p}} \frac{1}{2} \left[ (E_{\mathbf{p}+\mathbf{q}} + E_{\mathbf{p}}) \left( 1 - \frac{\xi_{\mathbf{p}+\mathbf{q}} \xi_{\mathbf{p}}}{E_{\mathbf{p}+\mathbf{q}} E_{\mathbf{p}}} \right) + i\omega_n \left( \frac{\xi_{\mathbf{p}+\mathbf{q}}}{E_{\mathbf{p}+\mathbf{q}}} - \frac{\xi_{\mathbf{p}}}{E_{\mathbf{p}}} \right) \right] \frac{1 + n_{\mathbf{p}+\mathbf{q}} + n_{\mathbf{p}}}{\omega_n^2 + (E_{\mathbf{p}+\mathbf{q}} + E_{\mathbf{p}})^2}, \end{aligned} \quad (\text{E4})$$

where  $\xi_{\mathbf{p}} \equiv \varepsilon_{\mathbf{p}} + \Delta$ ,  $\Delta \equiv Un_0$ ,  $E_{\mathbf{p}} \equiv \sqrt{\varepsilon_{\mathbf{p}}(\varepsilon_{\mathbf{p}} + 2\Delta)}$ , and  $n_{\mathbf{p}} \equiv 1/(e^{E_{\mathbf{p}}/T} - 1)$ .

At  $T \geq T_c$ , the polarization functions are given by

$$\Pi_{11}(q) = - \sum_{\mathbf{p}} \frac{1 + n'_{\mathbf{p}+\mathbf{q}} + n'_{\mathbf{p}}}{\varepsilon_{\mathbf{p}+\mathbf{q}} + \varepsilon_{\mathbf{p}} + 2\Sigma_{11}(0) - 2\mu - i\omega_n}, \quad (\text{E5})$$

$$\Pi_{22}(q) = \sum_{\mathbf{p}} \frac{n'_{\mathbf{p}+\mathbf{q}} - n'_{\mathbf{p}}}{\varepsilon_{\mathbf{p}+\mathbf{q}} - \varepsilon_{\mathbf{p}} - i\omega_n}, \quad (\text{E6})$$

where  $n'_{\mathbf{p}} = 1/\{e^{[\varepsilon_{\mathbf{p}} + \Sigma_{11}(0) - \mu]/T} - 1\}$ .

- 
- [1] A. Abrikosov, L. Gorkov, and I. Dzyaloshinski, *Methods of Quantum Field Theory in Statistical Physics*, Dover Books on Physics Series (Dover Publications, 1975).
  - [2] D. Pines and P. Nozières, *The Theory of Quantum Liquids: Normal Fermi liquids*, Advanced book classics (W.A. Benjamin, 1966).
  - [3] P. Nozières and D. Pines, *The Theory of Quantum Liquids: Superfluid Bose liquids*, Advanced book classics (Addison-Wesley, 1990).
  - [4] G. D. Mahan, *Many-Particle Physics*, Physics of Solids and Liquids (Springer US, 2000).
  - [5] A. Griffin, *Excitations in a Bose-condensed Liquid*, Cambridge Classical Studies (Cambridge University Press, 1993).
  - [6] B. D. Josephson, Relation between the superfluid density and order parameter for superfluid He near  $T_c$ , *Physics Letters* **21**, 608 (1966).
  - [7] M. Holzmann and G. Baym, Condensate superfluidity and infrared structure of the single-particle Green's function: The Josephson relation, *Physical Review B* **76**, 092502 (2007).
  - [8] M. Ueda, *Fundamentals and New Frontiers of Bose-Einstein Condensation* (World Scientific, 2010).
  - [9] J. Gavoret and P. Nozières, Structure of the perturbation expansion for the bose liquid at zero temperature, *Annals of Physics* **28**, 349 (1964).
  - [10] L. Pitaevskii and S. Stringari, *Bose-Einstein Condensation and Superfluidity*, International Series of Monographs on Physics (OUP Oxford, 2016).
  - [11] E. P. Gross, Structure of a quantized vortex in boson systems, *Il Nuovo Cimento* (1955-1965) **20**, 454 (1961).
  - [12] L. P. Pitaevskii, Vortex Lines in an Imperfect Bose Gas, *Zh. Eksp. Teor. Fiz.* **40**, 646 (1961).

- [13] N. N. Bogolyubov, On the theory of superfluidity, J. Phys.(USSR) **11**, 23 (1947).
- [14] A. L. Gaunt, T. F. Schmidutz, I. Gotlibovych, R. P. Smith, and Z. Hadzibabic, Bose-Einstein Condensation of Atoms in a Uniform Potential, Physical Review Letters **110**, 200406 (2013).
- [15] A. J. Leggett, Bose-Einstein condensation in the alkali gases: Some fundamental concepts, Rev. Mod. Phys. **73**, 307 (2001).
- [16] F. Dalfovo, S. Giorgini, L. P. Pitaevskii, and S. Stringari, Theory of Bose-Einstein condensation in trapped gases, Rev. Mod. Phys. **71**, 463 (1999).
- [17] H. T. C. Stoof, K. B. Gubbels, and D. B. M. Dickerscheid, *Ultracold Quantum Fields*, Theoretical and Mathematical Physics (Springer Netherlands, 2008).
- [18] C. W. Gardiner and P. Zoller, *The Quantum World of Ultra-Cold Atoms and Light Book III: Ultra-Cold Atoms*, Cold Atoms, Vol. 05 (WORLD SCIENTIFIC (EUROPE), 2017).
- [19] C. Chin, R. Grimm, P. Julienne, and E. Tiesinga, Feshbach resonances in ultracold gases, Reviews of Modern Physics **82**, 1225 (2010).
- [20] M. R. Andrews, D. M. Kurn, H. J. Miesner, D. S. Durfee, C. G. Townsend, S. Inouye, and W. Ketterle, Propagation of Sound in a Bose-Einstein Condensate, Physical Review Letters **79**, 553 (1997).
- [21] J. Stenger, S. Inouye, A. P. Chikkatur, D. M. Stamper-Kurn, D. E. Pritchard, and W. Ketterle, Bragg Spectroscopy of a Bose-Einstein Condensate, Physical Review Letters **82**, 4569 (1999).
- [22] D. M. Stamper-Kurn, A. P. Chikkatur, A. Gorlitz, S. Inouye, S. Gupta, D. E. Pritchard, and W. Ketterle, Excitation of Phonons in a Bose-Einstein Condensate by Light Scattering, Physical Review Letters **83**, 2876 (1999).
- [23] J. Steinhauer, R. Ozeri, N. Katz, and N. Davidson, Excitation Spectrum of a Bose-Einstein Condensate, Physical Review Letters **88**, 120407 (2002).
- [24] S. B. Papp, J. M. Pino, R. J. Wild, S. Ronen, C. E. Wieman, D. S. Jin, and E. A. Cornell, Bragg Spectroscopy of a Strongly Interacting  $^{85}\text{Rb}$  Bose-Einstein Condensate, Physical Review Letters **101**, 135301 (2008).
- [25] P. Navez, Manifestation of a gap due to the exchange energy in a spinor condensate, Physica A: Statistical Mechanics and its Applications **387**, 4070 (2008).
- [26] P. Navez and K. Bongs, Gap and screening in Raman scattering of a Bose condensed gas, EPL (Europhysics Letters) **88**, 60008 (2010).

- [27] T. Kita, Exact results on the two-particle Green's function of a Bose-Einstein condensate, *Physical Review B* **81**, 214513 (2010).
- [28] T. Kita, Properties of Nambu–Goldstone Bosons in a Single-Component Bose–Einstein Condensate, *Journal of the Physical Society of Japan* **80**, 084606 (2011).
- [29] T. Kita, Effective Action for Bose–Einstein Condensates, *Journal of the Physical Society of Japan* **83**, 064005 (2014).
- [30] T. Kita, A Renormalization-Group Study of Interacting Bose–Einstein Condensates: Absence of the Bogoliubov Mode below Four ( $T > 0$ ) and Three ( $T = 0$ ) Dimensions, *Journal of the Physical Society of Japan* **88**, 054003 (2019).
- [31] K. Tsutsui and Y. Kato, Are Quasiparticles and Phonons Identical in Bose–Einstein Condensates?, *Journal of the Physical Society of Japan* **85**, 124004 (2016).
- [32] Y. Nambu, Quasi-Particles and Gauge Invariance in the Theory of Superconductivity, *Physical Review* **117**, 648 (1960).
- [33] J. R. Schrieffer, *Theory of Superconductivity*, *Frontiers in physics* (W.A. Benjamin, 1964).
- [34] S. Watabe, Hidden multiparticle excitation in a weakly interacting Bose–Einstein condensate, *Physical Review* **97**, 033606 (2018).
- [35] A. A. N. Nepomnyashchii and Y. A, Contribution to the theory of the spectrum of a Bose system with condensate at small momenta, *Pis'ma Zh. Eksp. Teor. Fiz.* **21**, 3 (1975).
- [36] Y. A. N. Nepomnyashchii and A. A, Infrared divergence in field theory of a Bose system with a condensate, *Zh. Eksp. Teor. Fiz.* **75**, 976 (1978).
- [37] S. Watabe and Y. Ohashi, Comparative studies of many-body corrections to an interacting Bose-Einstein condensate, *Physical Review A* **88**, 053633 (2013).
- [38] S. Watabe and Y. Ohashi, Green's-function formalism for a condensed Bose gas consistent with infrared-divergent longitudinal susceptibility and Nepomnyashchii-Nepomnyashchii identity, *Physical Review A* **90**, 013603 (2014).
- [39] S. Watabe, Identities and Many-Body Approaches in Bose-Einstein Condensates, *Acta Physica Polonica A* **135**, 1222 (2019).
- [40] P. C. Hohenberg and P. C. Martin, Microscopic theory of superfluid helium, *Annals of Physics* **34**, 291 (1965).
- [41] N. M. Hugenholtz and D. Pines, Ground-State Energy and Excitation Spectrum of a System of Interacting Bosons, *Physical Review* **116**, 489 (1959).

- [42] V. N. Popov and A. V. Seredniakov, Low-frequency asymptotic form of the self-energy parts of a superfluid Bose system at  $T = 0$ , Zh. Eksp. Teor. Fiz. **77**, 377 (1979).
- [43] Y. A. Nepomnyashchii, Concerning the nature of the  $\lambda$ -transition order parameter, Zh. Eksp. Teor. Fiz. **85**, 1244 (1983).
- [44] P. B. Weichman, Crossover scaling in a dilute bose superfluid near zero temperature, Physical Review B **38**, 8739 (1988).
- [45] S. Giorgini, L. Pitaevskii, and S. Stringari, Bose-Einstein condensation, phase fluctuations, and two-phonon effects in superfluid  $^4\text{He}$ , Physical Review B **46**, 6374 (1992).
- [46] V. N. Popov, *Functional Integrals in Quantum Field Theory and Statistical Physics*, Mathematical Physics and Applied Mathematics (Springer Netherlands, 2001).
- [47] N. Dupuis, Infrared behavior in systems with a broken continuous symmetry: Classical O(N) model versus interacting bosons, Phys Rev E **83**, 031120 (2011).
- [48] H. T. C. Stoof and J. J. R. M. van Heugten, Resummation of Infrared Divergencies in the Theory of Atomic Bose Gases, Journal of Low Temperature Physics **174**, 159 (2013).
- [49] K. Huang and A. Klein, Phonons in liquid helium, Annals of Physics **30**, 203 (1964).
- [50] N. Dupuis and A. Rançon, Infrared behavior of interacting bosons at zero temperature, Laser Physics **21**, 1470 (2011).
- [51] D. Podolsky, A. Auerbach, and D. P. Arovas, Visibility of the amplitude (Higgs) mode in condensed matter, Physical Review B **84**, 174522 (2011).
- [52] A. D. B. Woods, Neutron Inelastic Scattering from Liquid Helium at Small Momentum Transfers, Physical Review Letters **14**, 355 (1965).
- [53] E. R. Pike, J. M. Vaughan, and W. F. Vinen, Brillouin scattering from superfluid  $^4\text{He}$ , Journal of Physics C: Solid State Physics **3**, L40 (1970).
- [54] A. D. B. Woods and R. A. Cowley, Structure and excitations of liquid helium, Reports on Progress in Physics **36**, 1135 (1973).
- [55] A. D. B. Woods and E. C. Svensson, Temperature Dependence of  $S(Q, \omega)$  in Superfluid  $^4\text{He}$ , Physical Review Letters **41**, 974 (1978).
- [56] E. F. Talbot, H. R. Glyde, W. G. Stirling, and E. C. Svensson, Temperature dependence of  $S(Q, \omega)$  in liquid  $^4\text{He}$  under pressure, Phys. Rev. B **38**, 11229 (1988).
- [57] W. G. Stirling and H. R. Glyde, Temperature dependence of the phonon and roton excitations in liquid  $^4\text{He}$ , Physical Review B **41**, 4224 (1990).

- [58] B. Fåk and K. H. Andersen, Neutron inelastic scattering from superfluid  $^4\text{He}$  beyond the roton minimum, *Physics Letters A* **160**, 468 (1991).
- [59] G. Winterling, F. S. Holmes, and T. J. Greytak, Light Scattering from First and Second Sound near the  $\lambda$  Transition in Liquid He, *Physical Review Letters* **30**, 427 (1973).
- [60] J. A. Tarvin, F. Vidal, and T. J. Greytak, Measurements of the dynamic structure factor near the lambda temperature in liquid helium, *Phys. Rev. B* **15**, 4193 (1977).
- [61] A. Miller, D. Pines, and P. Nozières, Elementary Excitations in Liquid Helium, *Phys. Rev.* **127**, 1452 (1962).
- [62] A. Griffin, Density fluctuation spectrum of superfluid  $^4\text{He}$  at finite temperatures, *Phys. Rev. B* **19**, 5946 (1979).
- [63] A. Griffin, Structure of the static pair-correlation function in superfluid  $^4\text{He}$ , *Phys. Rev. B* **22**, 5193 (1980).
- [64] A. Griffin, High- and low-frequency behavior of response functions in a Bose condensed liquid, *Journal of Low Temperature Physics* **44**, 441 (1981).
- [65] H. R. Glyde, Neutron scattering from liquid  $^4\text{He}$ , *Journal of Low Temperature Physics* **87**, 407 (1992).
- [66] H. R. Glyde, Density and quasiparticle excitations in liquid  $^4\text{He}$ , *Physical Review B* **45**, 7321 (1992).
- [67] H. R. Glyde, Quasiparticle Excitations, Bose Condensation, and the f-Sum Rule, *Physical Review Letters* **75**, 4238 (1995).
- [68] S. O. Diallo, R. T. Azuah, D. L. Abernathy, J. Taniguchi, M. Suzuki, J. Bossy, N. Mulders, and H. R. Glyde, Evidence for a Common Physical Origin of the Landau and BEC Theories of Superfluidity, *Physical Review Letters* **113**, 215302 (2014).
- [69] M. Cohen and R. P. Feynman, Theory of Inelastic Scattering of Cold Neutrons from Liquid Helium, *Phys. Rev.* **107**, 13 (1957).
- [70] E. Manousakis and V. R. Pandharipande, Theoretical studies of the dynamic structure function of liquid  $^4\text{He}$ , *Physical Review B* **33**, 150 (1986).
- [71] A. Griffin and E. C. Svensson, New interpretation of the quasiparticle weight  $Z(Q)$  for superfluid  $^4\text{He}$ , *Physica B: Physics of Condensed Matter* **165-166**, 487 (1990).
- [72] E. Talbot and A. Griffin, Theory of neutron scattering from superfluid  $^4\text{He}$  at finite temperatures, *Physical Review B* **29**, 2531 (1984).



- [73] P. C. Hohenberg and P. C. Martin, Superfluid Dynamics in the Hydrodynamic ( $\omega\tau \ll 1$ ) and Collisionless ( $\omega\tau \gg 1$ ) Domains, *Physical Review Letters* **12**, 69 (1964).
- [74] T. H. Cheung and A. Griffin, Density Fluctuations in an Interacting Bose Gas, *Physical Review A* **4**, 237 (1971).
- [75] W. Götze and M. Lücke, Dynamical structure factor  $S(q, \omega)$  of liquid helium II at zero temperature, *Physical Review B* **13**, 3825 (1976).
- [76] P. C. Hohenberg, E. D. Siggia, and B. I. Halperin, Density-correlation function for liquid helium near  $T_\lambda$  in the symmetric planar-spin model, *Physical Review B* **14**, 2865 (1976).
- [77] W. Götze and M. Lücke, Self-consistent second-order approximation for the liquid-helium-II excitation spectrum, *Physical Review B* **13**, 3822 (1976).
- [78] H. Kang, Equivalent wave-function approach to the  $^4\text{He}$  structure factor and excitation spectrum, *Physical Review B* **17**, 4287 (1978).
- [79] E. Talbot and A. Griffin, High- and low-frequency behaviour of response functions in a Bose liquid: One-loop approximation, *Annals of Physics* **151**, 71 (1983).
- [80] S. H. Payne and A. Griffin, Goldstone phonons in a Bose-condensed gas at finite temperature: One-loop approximation, *Physical Review B* **32**, 7199 (1985).
- [81] K. Fukushima and F. Iseki, Determination of the zeroth moment of the effective roton-maxon interaction in liquid He II, *Physical Review B* **38**, 4448 (1988).
- [82] H. R. Glyde and A. Griffin, Zero sound and atomiclike excitations: The nature of phonons and rotons in liquid  $^4\text{He}$ , *Physical Review Letters* **65**, 1454 (1990).
- [83] A. Zawadowski, J. Ruvalds, and J. Solana, Bound Roton Pairs in Superfluid Helium, *Physical Review A* **5**, 399 (1972).
- [84] S. Stringari, Sum rules for density and particle excitations in Bose superfluids, *Physical Review B* **46**, 2974 (1992).
- [85] Y. A. Nepomnyashchy, Nature of excitations in liquid  $^4\text{He}$ , *Phys. Rev. B* **46**, 6611 (1992).
- [86] A. Griffin and T. H. Cheung, Excitations in a Bose Gas at Finite Temperatures. II. Relation between Single-Particle and Density Fluctuations, *Physical Review A* **7**, 2086 (1973).
- [87] M. Fliesser, J. Reidl, P. Szépfalusy, and R. Graham, Conserving and gapless model of the weakly interacting Bose gas, *Physical Review A* **64**, 013609 (2001).
- [88] A. J. Leggett and D. ter Haar, Finite Linewidths and "Forbidden" Three-Phonon Interactions, *Physical Review* **139**, A779 (1965).

- [89] C. J. Pethick and D. ter Haar, On the attenuation of sound in liquid helium, *Physica* **32**, 1905 (1966).
- [90] S. Sunakawa, S. Yamasaki, and T. Kebukawa, Energy Spectrum of the Excitations in Liquid Helium II, *Progress of Theoretical Physics* **41**, 919 (1969).
- [91] T. Kebukawa, S. Yamasaki, and S. Sunakawa, On the Excitation Energy in Liquid Helium II, *Progress of Theoretical Physics* **44**, 565 (1970).
- [92] T. Kebukawa, The Temperature Dependence of Phonon Velocity and Roton Minimum in Liquid He II, *Progress of Theoretical Physics* **49**, 388 (1973).
- [93] G. W. Goble and D. H. Kobe, Microscopic calculation of the excitation spectrum of superfluid helium-4, *Physical Review A* **10**, 851 (1974).
- [94] J. Prakash and K. K. Singh, Temperature Dependence of Quasi-Particle Sound Velocity in a Bose gas, *Lett. Nuovo Cimento* **19**, 377 (1977).
- [95] K. K. Singh and J. Prakash, Temperature dependence of quasiparticle sound velocity in a Bose gas, *Physical Review B* **17**, 1253 (1978).
- [96] R. A. Ferrell and J. K. Bhattacharjee, Dynamic Scaling of Ultrasonic Attenuation at the Liquid Helium  $\lambda$  Point, *Physical Review Letters* **44**, 403 (1980).
- [97] R. A. Ferrell and J. K. Bhattacharjee, Sound propagation in liquid helium near the lambda point: Thermodynamics, *Physical Review B* **25**, 3168 (1982).
- [98] C.-I. Um, W.-H. Kahng, K.-H. Yeon, S.-T. Choh, and A. Isihara, Temperature variation of sound velocity in liquid He II, *Physical Review B* **29**, 5203 (1984).
- [99] A. F. Andreev and I. M. Khalatnikov, Sound in liquid helium II near absolute zero, *Sov. Phys. JETP* **17**, 1384 (1963).
- [100] I. M. Khalatnikov and D. M. Chernikova, Dispersion of First and Second Sound in Superfluid Helium, *Sov. Phys. JETP* **23**, 274 (1966).
- [101] R. A. Ferrell, N. Menyhárd, H. Schmidt, F. Schwabl, and P. Szépfalusy, Fluctuations and lambda phase transition in liquid helium, *Annals of Physics* **47**, 565 (1968).
- [102] A. F. Andreev and I. M. Khalatnikov, On the temperature dependence of the velocity of sound in liquid helium, *Journal of Low Temperature Physics* **2**, 173 (1970).
- [103] T. Kebukawa, Temperature Dependence of the Absorption Coefficient of First Sound and Its Velocity in Liquid Helium II, *Progress of Theoretical Physics* **51**, 366 (1974).
- [104] R. A. Ferrell and J. K. Bhattacharjee, Critical ultrasonic attenuation in superfluid helium:

- Mixing of order-parameter and fluctuation contributions, *Physical Review B* **23**, 2434 (1981).
- [105] R. A. Ferrell, B. Mirhashem, and J. K. Bhattacharjee, Sound propagation in liquid helium near the  $\lambda$  point. II. Ultrasonic attenuation, *Physical Review B* **35**, 4662 (1987).
  - [106] S. Sunakawa, Y. Yoko-o, and H. Nakatani, Collective Description of a System of Interacting Bose Particles. I, *Progress of Theoretical Physics* **27**, 589 (1962).
  - [107] S. Sunakawa, H. Nakatani, and Y. Yoko-o, Collective Description of a System of Interacting Bose Particles. II, *Progress of Theoretical Physics* **27**, 600 (1962).
  - [108] S. Sunakawa, Y. Yoko-o, and H. Nakatani, On the Phonon-Phonon Interaction in a System of Bose Particles, *Progress of Theoretical Physics* **28**, 127 (1962).
  - [109] T. Nishiyama, Method of Collective Description of the Excitations in Liquid Helium, *Progress of Theoretical Physics* **45**, 730 (1971).
  - [110] S. Yamasaki, T. Kebukawa, and S. Sunakawa, On the Collective Variables in Many-Boson System, *Progress of Theoretical Physics* **53**, 1243 (1975).
  - [111] H. J. Maris, Hydrodynamics of Superfluid Helium below 0.6°K. II. Velocity and Attenuation of Ultrasonic Waves, *Physical Review A* **8**, 2629 (1973).
  - [112] J. C. Findlay, A. Pitt, H. G. Smith, and J. O. Wilhelm, The Velocity of Sound in Liquid Helium, *Physical Review* **54**, 506 (1938).
  - [113] K. R. Atkins and C. E. Chase, The Velocity of First Sound in Liquid Helium, *Proceedings of the Physical Society. Section A* **64**, 826 (1951).
  - [114] C. E. Chase and D. Shoenberg, Ultrasonic measurements in liquid helium, *Proceedings of the Royal Society of London. Series A. Mathematical and Physical Sciences* **220**, 116 (1953).
  - [115] A. Van Itterbeek and G. Forrez, First sound measurements in liquid helium, *Physica* **20**, 133 (1954).
  - [116] J. R. Pellam and C. F. Squire, Ultrasonic Velocity and Absorption in Liquid Helium, *Physical Review* **72**, 1245 (1947).
  - [117] C. E. Chase, Propagation of Ordinary Sound in Liquid Helium near the  $\lambda$  Point, *Physics of Fluids* **1**, 193 (1958).
  - [118] W. M. Whitney and C. E. Chase, Velocity of Sound in Liquid Helium at Low Temperatures, *Physical Review Letters* **9**, 243 (1962).
  - [119] C. E. Chase, R. C. Williamson, and L. Tisza, Ultrasonic Propagation Near the Critical Point in Helium, *Physical Review Letters* **13**, 467 (1964).

- [120] W. M. Whitney and C. E. Chase, Ultrasonic Velocity and Dispersion in Liquid Helium II from 0.15 to 1.8°K, *Physical Review* **158**, 200 (1967).
- [121] B. M. Abraham, Y. Eckstein, J. B. Ketterson, M. Kuchnir, and J. Vignos, Sound Propagation in Liquid  $^4\text{He}$ , *Physical Review* **181**, 347 (1969).
- [122] B. N. Esel'son, M. I. Kaganov, E. Y. Rudavskii, and I. A. Serbin, "Sound" in superfluid liquids, *Sov. Phys. Usp.* **17**, 215 (1974).
- [123] J. Maza, F. Miguelez, A. Veira, and F. Vidal, The velocity of sound in liquid helium near the lambda point, *Journal of Physics C: Solid State Physics* **21**, L75 (1988).
- [124] K. R. Atkins, *Liquid Helium*, Cambridge monographs on physics (University Press, 1959).
- [125] W. A. Jeffers and W. M. Whitney, Temperature and Frequency Dependence of Ultrasonic Absorption in Liquid Helium below 1°K, *Physical Review* **139**, A1082 (1965).
- [126] O. V. Lounasmaa, Pressure Coefficient and Compressibility of Liquid  $\text{He}^4$  Very Close to the  $\lambda$  Curve, *Physical Review* **130**, 847 (1963).
- [127] C. Simanta and S. J. Yatendra, (2006), arXiv:cond-mat/0612279.
- [128] K. B. Davis, M. O. Mewes, M. R. Andrews, N. J. van Druten, D. S. Durfee, D. M. Kurn, and W. Ketterle, Bose-Einstein Condensation in a Gas of Sodium Atoms, *Physical Review Letters* **75**, 3969 (1995).
- [129] M. H. Anderson, J. R. Ensher, M. R. Matthews, C. E. Wieman, and E. A. Cornell, Observation of Bose-Einstein Condensation in a Dilute Atomic Vapor, *Science* **269**, 198 (1995).
- [130] R. Ozeri, N. Katz, J. Steinhauer, and N. Davidson, Colloquium: Bulk Bogoliubov excitations in a Bose-Einstein condensate, *Rev. Mod. Phys.* **77**, 187 (2005).
- [131] A. Brunello, F. Dalfovo, L. Pitaevskii, and S. Stringari, How to Measure the Bogoliubov Quasiparticle Amplitudes in a Trapped Condensate, *Physical Review Letters* **85**, 4422 (2000).
- [132] J. M. Vogels, K. Xu, C. Raman, J. R. Abo-Shaeer, and W. Ketterle, Experimental Observation of the Bogoliubov Transformation for a Bose-Einstein Condensed Gas, *Physical Review Letters* **88**, 060402 (2002).
- [133] R. Mottl, F. Brennecke, K. Baumann, R. Landig, T. Donner, and T. Esslinger, Roton-Type Mode Softening in a Quantum Gas with Cavity-Mediated Long-Range Interactions, *Science* **336**, 1570 (2012).
- [134] S.-C. Ji, L. Zhang, X.-T. Xu, Z. Wu, Y. Deng, S. Chen, and J.-W. Pan, Softening of Roton and Phonon Modes in a Bose-Einstein Condensate with Spin-Orbit Coupling, *Physical Review*

- Letters **114**, 105301 (2015).
- [135] L.-C. Ha, L. W. Clark, C. V. Parker, B. M. Anderson, and C. Chin, Roton-Maxon Excitation Spectrum of Bose Condensates in a Shaken Optical Lattice, *Physical Review Letters* **114**, 055301 (2015).
  - [136] D. Petter, G. Natale, R. M. W. van Bijnen, A. Patscheider, M. J. Mark, L. Chomaz, and F. Ferlaino, Probing the Roton Excitation Spectrum of a Stable Dipolar Bose Gas, *Physical Review Letters* **122**, 183401 (2019).
  - [137] J. L. Ville, R. Saint-Jalm, É. Le Cerf, M. Aidelsburger, S. Nascimbène, J. Dalibard, and J. Beugnon, Sound Propagation in a Uniform Superfluid Two-Dimensional Bose Gas, *Physical Review Letters* **121**, 145301 (2018).
  - [138] S. J. Garratt, C. Eigen, J. Zhang, P. Turzák, R. Lopes, R. P. Smith, Z. Hadzibabic, and N. Navon, From single-particle excitations to sound waves in a box-trapped atomic Bose-Einstein condensate, *Physical Review* **99**, 021601 (2019).
  - [139] T. Kita, Self-consistent perturbation expansion for Bose-Einstein condensates satisfying Goldstone's theorem and conservation laws, *Physical Review B* **80**, 214502 (2009).
  - [140] T. Kita, A Renormalization-Group Study of Interacting Bose-Einstein Condensates: II. Anomalous Dimension  $\eta$  for  $d \lesssim 4$  at Finite Temperatures, *Journal of the Physical Society of Japan* **88**, 104003 (2019).
  - [141] P. C. Hohenberg and P. C. Martin, Microscopic Theory of Superfluid Helium, *Annals of Physics* **34**, 291 (1965).
  - [142] A. Griffin, Conserving and gapless approximations for an inhomogeneous Bose gas at finite temperatures, *Physical Review B* **53**, 9341 (1996).
  - [143] V. I. Yukalov, Representative statistical ensembles for Bose systems with broken gauge symmetry, *Annals of Physics* **323**, 461 (2008).
  - [144] V. I. Yukalov, Basics of Bose-Einstein condensation, *Physics of Particles and Nuclei* **42**, 460 (2011).
  - [145] P. Kopietz, L. Bartosch, and F. Schütz, *Introduction to the Functional Renormalization Group* (Springer, 2010).
  - [146] A. Sinner, N. Hasselmann, and P. Kopietz, Functional renormalization-group approach to interacting bosons at zero temperature, *Physical Review A* **82**, 063632 (2010).
  - [147] G. Baym, The Microscopic Description of Superfluidity, in *Mathematical Methods in Solid*

- State and Superfluid Theory: Scottish Universities' Summer School*, edited by R. C. Clark and G. H. Derrick (Springer US, Boston, MA, 1968) pp. 121–156.
- [148] M. Holzmann and G. Baym, Condensate Density and Superfluid Mass Density of a Dilute Bose-Einstein Condensate near the Condensation Transition, *Physical Review Letters* **90**, 040402 (2003).
  - [149] V. I. Yukalov, Theory of cold atoms: Bose–Einstein statistics, *Laser Physics* **26**, 062001 (2016).
  - [150] D. Forster, *Hydrodynamic Fluctuations, Broken Symmetry, And Correlation Functions* (CRC Press, 2018).
  - [151] K. Fukushima and F. Iseki, Determination of the zeroth moment of the effective roton-maxon interaction in liquid He II, *Physical Review B* **38**, 4448 (1988).
  - [152] V. N. Popov and L. D. Faddeev, An Approach to the theory of the low-temperature Bose gas, *Zh. Eksp. Teor. Fiz.* **47**, 1315 (1964).
  - [153] V. N. Popov, Green Functions and Thermodynamic Functions of a Non-ideal Bose Gas, *Zh. Eksp. Teor. Fiz.* **47**, 1759 (1965).
  - [154] H. Shi and A. Griffin, Finite-temperature excitations in a dilute Bose-condensed gas, *Physics Reports* **304**, 1 (1998).
  - [155] N. Shohno, Low-Temperature Properties of the Interacting Bose System, *Progress of Theoretical Physics* **31**, 553 (1964).
  - [156] V. N. Popov, Hydrodynamic Hamiltonian for a nonideal Bose gas, *Teoreticheskaya i Matematicheskaya Fizika* **11**, 236 (1972).
  - [157] M. Bijlsma and H. T. C. Stoof, Renormalization group theory of the three-dimensional dilute Bose gas, *Physical Review A* **54**, 5085 (1996).
  - [158] A. Sinner, N. Hasselmann, and P. Kopietz, Spectral Function and Quasiparticle Damping of Interacting Bosons in Two Dimensions, *Physical Review Letters* **102**, 120601 (2009).
  - [159] O. Hryhorchak and V. Pastukhov, Large- $N$  properties of a non-ideal Bose gas, *Journal of Physics A: Mathematical and Theoretical* **52**, 025002 (2018).
  - [160] F. Marsiglio, M. Schossmann, and J. P. Carbotte, Iterative analytic continuation of the electron self-energy to the real axis, *Phys. Rev. B* **37**, 4965 (1988).
  - [161] Y. Takada and T. Higuchi, Vertex function for the coupling of an electron with intramolecular phonons: Exact results in the antiadiabatic limit, *Phys. Rev. B* **52**, 12720 (1995).

- [162] B. Capogrosso-Sansone, S. Giorgini, S. Pilati, L. Pollet, N. Prokof'ev, B. Svistunov, and M. Troyer, The Beliaev technique for a weakly interacting Bose gas, *New Journal of Physics* **12**, 043010 (2010).
- [163] Y. Kawaguchi and M. Ueda, Spinor Bose–Einstein condensates, *Physics Reports* **520**, 253 (2012).
- [164] M. Baranov, Theoretical progress in many-body physics with ultracold dipolar gases, *Physics Reports* **464**, 71 (2008).
- [165] M. Ota, F. Larcher, F. Dalfovo, L. Pitaevskii, N. P. Proukakis, and S. Stringari, Collisionless Sound in a Uniform Two-Dimensional Bose Gas, *Physical Review Letters* **121**, 145302 (2018).
- [166] J. Hofmann and W. Zwerger, Deep Inelastic Scattering on Ultracold Gases, *Physical Review X* **7**, 011022 (2017).
- [167] A. Camacho-Guardian and G. M. Bruun, Landau Effective Interaction between Quasiparticles in a Bose-Einstein Condensate, *Physical Review X* **8**, 031042 (2018).